Ferroelasticity, anelasticity and magnetoelastic relaxation in Co-doped iron pnictide: $Ba(Fe_{0.957}Co_{0.043})_2As_2$

OPEN ACCESS
IOP Publishing
Journal of Physics: Condensed Matter
J. Phys.: Condens. Matter **31** (2019) 155401 (22pp)
https://doi.org/10.1088/1361-648X/aafe29

Ferroelasticity, anelasticity and magnetoelastic relaxation in Co-doped iron pnictide: $Ba(Fe_{0.957}Co_{0.043})_2As_2$

M A Carpenter[1,7], D M Evans[1,2], J A Schiemer[1], T Wolf[3], P Adelmann[3], A E Böhmer[3,4], C Meingast[3], S E Dutton[5], P Mukherjee[5] and C J Howard[6]

[1] Department of Earth Sciences, University of Cambridge, Downing Street, Cambridge CB2 3EQ, United Kingdom
[2] Department of Materials Science and Engineering, Norwegian University of Science and Technology, 7491 Trondheim, Norway
[3] Institut für Festkörperphysik, Karlsruhe Institute of Technology, 76021 Karslruhe, Germany
[4] Ames Laboratory, U.S. Department of Energy, Ames, IA 50011, United States of America
[5] Cavendish Laboratory, University of Cambridge, Madingley Road, Cambridge CB3 0HE, United Kingdom
[6] School of Engineering, University of Newcastle, Callaghan NSW 2308, Australia

E-mail: mc43@esc.cam.ac.uk

Received 15 October 2018, revised 19 December 2018
Accepted for publication 14 January 2019
Published 15 February 2019

Abstract

The hypothesis that strain has a permeating influence on ferroelastic, magnetic and superconducting transitions in 122 iron pnictides has been tested by investigating variations of the elastic and anelastic properties of a single crystal of $Ba(Fe_{0.957}Co_{0.043})_2As_2$ by resonant ultrasound spectroscopy as a function of temperature and externally applied magnetic field. Non-linear softening and stiffening of C_{66} in the stability fields of both the tetragonal and orthorhombic structures has been found to conform quantitatively to the Landau expansion for a pseudoproper ferroelastic transition which is second order in character. The only exception is that the transition occurs at a temperature ($T_S \approx 69$ K) ~10 K above the temperature at which C_{66} would extrapolate to zero ($T^*_{cE} \approx 59$ K). An absence of anomalies associated with antiferromagnetic ordering below $T_N \approx 60$ K implies that coupling of the magnetic order parameter with shear strain is weak. It is concluded that linear-quadratic coupling between the structural/electronic and antiferromagnetic order parameters is suppressed due to the effects of local heterogeneous strain fields arising from the substitution of Fe by Co. An acoustic loss peak at ~50–55 K is attributed to the influence of mobile ferroelastic twin walls that become pinned by a thermally activated process involving polaronic defects. Softening of C_{66} by up to ~6% below the normal—superconducting transition at $T_c \approx 13$ K demonstrates an effective coupling of the shear strain with the order parameter for the superconducting transition which arises indirectly as a consequence of unfavourable coupling of the superconducting order parameter with the ferroelastic order parameter. $Ba(Fe_{0.957}Co_{0.043})_2As_2$ is representative of 122 pnictides as forming a class of multiferroic superconductors in which elastic strain relaxations

[7] Author to whom any correspondence should be addressed.

underpin almost all aspects of coupling between the structural, magnetic and superconducting order parameters and of dynamic properties of the transformation microstructures they contain.

Keywords: pnictide, magnetoelastic coupling, strain relaxation, ferroelastic twin walls, superconductivity

(Some figures may appear in colour only in the online journal)

1. Introduction

Materials with multiple instabilities are of topical interest both for the complex physics they display and for opportunities they provide in relation to the tuning of physical properties in potential device applications. They may combine, for example, ferroelectricity, (anti)ferromagnetism and ferroelasticity in multiferroics, magnetism and martensitic instabilities in magnetocalorics and shape memory alloys, or magnetism, ferroelasticity and superconductivity in unconventional superconductors. The primary focus tends to be on ranges of chemistry, structure and parameter space where two or more phase boundaries converge but, in any system with multiple instabilities, an important mechanism for coupling between the different order parameters is via common strains. This has consequences for the elastic properties even though they may not be the main properties of technological interest. In this context, the 122 pnictide $Ba(Fe_{1-x}Co_x)_2As_2$ is representative of multiferroic superconductors with three phase transitions. End-member $BaFe_2As_2$ undergoes a tetragonal to orthorhombic ferroelastic transition near ~135 K, followed by antiferromagnetic ordering ~0.5–1 K below this [1–4]. Doping with Co causes suppression of both transitions to lower temperatures until they meet a field of unconventional superconductivity, with the highest critical temperature occurring where the ferroelastic transition line meets the superconducting transition line [5–9].

Multiple instabilities also give rise to complex transformation microstructures on a mesoscopic length scale which have distinctive properties in their own right (e.g. [10–13]). Ferroelastic materials are particularly remarkable for the diversity of strain related twin walls, tweed and glassy behaviour they display [14]. For $Ba(Fe_{1-x}Co_x)_2As_2$ there are three distinct microstructures to consider: twin walls and tweed associated with the pseudoproper ferroelastic phase transition, magnetic domain walls and, in the presence of a magnetic field below the superconducting transition, vortices. If there is any strain contrast across them, the different microstructures will not only interact with each other but will also be susceptible to pinning by local strain fields. For example, it is already known that vortices in $Ba(Fe_{1-x}Co_x)_2As_2$ are repelled from ferroelastic twin walls [15] and that the best pinning conditions for a high critical current appear to occur when the twin walls are interwoven and closely spaced [16].

Here we present elastic and anelastic properties of a single crystal of $Ba(Fe_{0.957}Co_{0.043})_2As_2$ measured as a function of temperature and magnetic field using resonant ultrasound spectroscopy (RUS). The primary objective was to reveal the contributions of both static and dynamic strain coupling effects throughout the stability fields of both the tetragonal and orthorhombic phases. The composition was chosen so as to give three phase transitions which are closely spaced but with just sufficient separation that variations of the strain coupling behaviour associated with each could be distinguished. The wider significance is that features due to the pervasive role of strain coupling must occur also in other 122 and 1111 pnictides. Strain fields are long ranging interactions in a crystal. They not only give rise to coupling between different order parameters on a macroscopic length scale but also promote a strong tendency for the evolution of each order parameter to conform to mean field behaviour. For example, Karahasanovic and Schmalian [17] have shown how the coupling promotes mean field behaviour for the structural/electronic transition but does not influence the magnetic transition. Imposing a strain also provides a significant control on transport properties associated with the superconducting transition in $Ba(Fe_{1-x}Co_x)_2As_2$ thin films [18, 19].

The paper is divided into five main sections. Coupling between order parameters for the three phase transitions and their individual couplings with strain are introduced in section 2. A formal treatment of the relevant Landau expansion needed to derive expressions for the elastic constants is given separately in an appendix. In order to allow close correlation of elastic and anelastic anomalies from RUS with properties that are discussed more widely in the literature, extensive measurements of heat capacity and magnetism were undertaken on a second crystal, as introduced in section 3 and set out in the appendix. Primary RUS data showing the patterns of elastic softening associated with phase transitions as functions of temperature (2–300 K) and magnetic field (0–10 T) are given in section 4.

Elastic softening is due to strain/order parameter coupling so the formal analysis set out in section 5 starts with a determination of the spontaneous strain. This shows, firstly, that the ferroelastic transition is classically second order in character and, secondly, that coupling with the magnetic order parameter is weak or absent. Because of constraints arising from the small size and irregular shape of the crystal used for RUS measurements, separating the contributions of different single crystal elastic constants was not trivial. Nevertheless, it has been possible to identify the separate contributions of C_{66}, $\frac{1}{2}(C_{11}-C_{12})$ and C_{44}. The evolution of C_{66} in the stability field of the orthorhombic structure is consistent with a Landau description of bilinear coupling between shear strain

and the driving order parameter. It appears that the ferroelastic microstructure might be important in determining the bulk elastic properties in a 10 K interval below the first transition and that an anelestic loss peak is indicative of the contribution of mobile twin walls, which become pinned below ~50–55 K.

The implications of the observed elastic and anelastic anomalies are considered in detail in section 6. A more complete description of the strain relaxation behaviour of the superconducting phase, including the contribution of vortices, is presented elsewhere [20].

2. Strain and order parameter coupling

The conventional model for combined structural and magnetic transitions in $Ba(Fe_{1-x}Co_x)_2As_2$ is of two order parameters associated with two discrete transitions and linear-quadratic coupling between them [2, 21–24]. The structural/electronic transition is taken to be pseudoproper ferroelastic, i.e. with the shear strain e_6 arising by bilinear coupling to the driving order parameter [23, 24].

The ferroelastic transition involves the change in space group $I4/mmm$–$Fmmm$ and is driven by an order parameter, Q_E, which transforms as the symmetry of a gamma point irreducible representation, Γ_4^+. There has been some discussion about the microscopic mechanism but it appears either to be electronic or, at least, to have an electronic component [25–28]. The elastic constant C_{66} shows non-linear temperature dependence due to the coupling term $\lambda e_6 Q_E$, where Q_E is the order parameter and e_6 the symmetry-breaking shear strain [21, 27, 29–35]. Non-symmetry breaking strains, $(e_1 + e_2)$ and e_3 are expected to couple as $\lambda e_i Q_E^2$.

The antiferromagnetic structure has magnetic space group C_Amca and the order parameter for the transition from the parent $I4/mmm$ structure, Q_M, has the symmetry of the irreducible representation mX_2^+ [36, 37]. By itself, the magnetic transition would be improper ferroelastic, with coupling of non-zero strains as $\lambda e_i Q_M^2$ where $i = 1,2,3,6$.

The superconducting transition would not introduce a symmetry-breaking shear strain and is therefore co-elastic in the terminology of Salje [38]. A macroscopic order parameter for the superconducting phase with respect to the parent $I4/mmm$ structure, Q_{SC}, is expected to couple with non-symmetry breaking strains as $\lambda e_i Q_{SC}^2$ where $i = 1$–3, while coupling with e_6 will be of the form $\lambda e_6^2 Q_{SC}^2$. Coupling of individual order parameters with strains in these ways will lead to coupling between the three order parameters as, in lowest order, $\lambda Q_E Q_M^2$, $\lambda Q_M^2 Q_{SC}^2$ and $\lambda Q_E^2 Q_{SC}^2$.

Other systems with linear-quadratic coupling also show pseudoproper ferroelastic softening and magnetic ordering. In Fe_xO and MnO, the critical temperature for antiferromagnetic ordering is higher than the critical temperature for a structural instability but coupling leads to a single transition, with both order parameters then evolving together. Magnetic ordering intervenes before the structural transition can occur and the only influence of the structural instability is seen as softening of C_{44} [39, 40]. In the case of $Pr_{0.48}Ca_{0.52}MnO_3$, coupling is between order parameters representing cooperative Jahn–Teller distortions and charge ordering, with gradient coupling contributions leading to the stabilization of an incommensurate structure [41]. Antiferromagnetic ordering occurs at a lower temperature but has no impact on the shear strains or the shear modulus. A special feature of the pnictides which differs from these examples is that spin and electronic instabilities are so closely related that there is a 'chicken and egg problem' as to which provides the real driving mechanism for the structural transition [28].

While it is well understood that the bilinear coupling term $\lambda e_6 Q_E$ determines the distinctive pattern of elastic softening with falling temperature in the parent tetragonal structure, strong attenuation of acoustic waves in the orthorhombic structure [31, 42] and large contributions from mobile twin walls in static loading experiments [21] have meant that elastic and anelastic properties of the orthorhombic structure have not been fully characterized. Experience of diverse phase transitions in perovskites has shown that details of the acoustic loss can be seen more clearly by RUS [43], which therefore provides an ideal tool for testing models of both static and dynamic strain coupling behaviour.

3. Sample characterization

RUS and magnetic measurements were made on self-flux grown single crystals with composition $Ba(Fe_{0.957}Co_{0.043})_2As_2$ which came from the same batch (TWOX1128) as referred to in Böhmer [44] and as used by Böhmer *et al* [35]. Details of the synthesis method are given by Hardy *et al* [45, 46]. The Co content in samples from this batch was accurately determined by refinement of four-circle single crystal x-ray diffraction data. Extensive experimental data for single crystals with other Co contents prepared in the same way have been given by Hardy *et al* [47] (heat capacity) Meingast *et al* [48] (thermal expansion) and Böhmer *et al* [35] (shear modulus). The two crystals used in the present study had masses 19.9 mg (Crystal 1) and 1.6 mg (Crystal 2). Crystal 1 had a shape that was close to being a rectangular parallelepiped with dimensions ~$0.35 \times 3.2 \times 4.2\,mm^3$ and the large faces parallel to (0 0 1). Crystal 2 was also a thin, approximately rectangular parallelepiped, ~$0.047 \times 1.6 \times 3.2\,mm^3$, with the large faces parallel to (0 0 1). As set out below, both crystals had sharp superconducting transitions close to 13 K, implying that they were chemically homogeneous and had the same composition.

Thermal expansion measurements within the (0 0 1) plane on another sample from batch TWOX1128 revealed anomalies at 69, 60 and 13 K, which are taken to be the transition temperatures for the structural/electronic transition, T_S, the Néel point, T_N, and the normal—superconducting transition temperature, T_c, respectively. These values are consistent with data in the literature for samples with compositions in the range $x = 0.037$–0.05 [5, 6, 8, 34, 47–50].

The heat capacity of Crystal 2 was measured as a function of temperature with and without an applied magnetic field in a Quantum Design physical property measurement system (PPMS). Data collected in zero field and at 7.5 T are shown in figure A1 of the appendix. There are small anomalies at

~69 and ~60 K, consistent with second order transitions at the expected structural and magnetic transition temperatures. These did not change under the influence of the magnetic field. The steps in heat capacity, ΔC_p, at T_N and T_S are ~0.15 and ~0.25 J · mole^{-1} · K^{-1}, respectively.

DC magnetic measurements were made on Crystal 2 in a Quantum Design magnetic property measuring system (MPMS) XL squid magnetometer. Selected data are given in the appendix section A.2 and do not show any obvious anomalies on repeated heating and cooling through T_N or T_S. This is consistent with magnetic susceptibility data from the literature which indicate that the magnitude of any magnetic anomalies drops off steeply with increasing Co-content [8]. The normal—superconducting transition is seen as a steep anomaly near 13 K. Magnetic hysteresis loops collected at temperatures below T_c display the characteristic fishtail pattern of unconventional superconductors, as seen previously from crystals of Co-doped $BaFe_2As_2$ [50–53]. In addition, a weakly ferromagnetic component was detected at all temperatures above T_c (appendix figure A3). The weak ferromagnetic moments are most likely due to some discrete impurity phase or to local moments associated with Fe atoms, rather than ferromagnetic ordering of the pnictide phase itself.

AC magnetic measurements were made in a DC field of 20 Oe using the AC Measurement System option in a Quantum Design PPMS instrument at frequencies between 0.01 and 10 kHz. As shown in the appendix section A.3, no obvious anomalies were observed in either the real or imaginary components of the magnetic susceptibility, χ' and χ'', between ~15 and 100 K. A steep change in χ' was accompanied by a peak in χ'' between ~12 and 15 K, with a small dependence on frequency, marking the normal—superconducting transition.

4. Resonant ultrasound spectroscopy (RUS)

RUS involves the stimulation and measurement of acoustic resonances of small samples held lightly between piezoelectric transducers [54]. The squared values of resonance peak frequencies, f, scale with values of combinations of predominantly shear elastic constants in different proportions. The inverse mechanical quality factor, Q^{-1}, is a measure of acoustic loss and is taken as $\Delta f/f$, where Δf is the width at half maximum height of a given peak. In general, variations of f can be followed with a resolution of ~0.1% or better, but the best indicator of uncertainty is provided by the magnitude of noise in the final f^2 and Q^{-1} variations. RUS has previously been used to follow the evolution of C_{66} as a function of temperature in single crystals of $Ba(Fe_{1-x}Co_x)_2As_2$ with $x = 0$ and 0.08 [29].

Spectra were collected using purpose-built electronics produced by Migliori in Los Alamos, with a maximum applied voltage of 2 V. The sample holder, as described by McKnight *et al* [55] but with the steel component replaced by copper [56], was placed within an Oxford Instruments Teslatron cryostat which has a superconducting magnet capable of delivering a magnetic field up to 14 T [56, 57]. Crystal 1 was mounted with the transducers resting lightly across the large faces so that the magnetic field was applied parallel to the crystallographic c-axis ($H//c$). As part of the experimental protocol, the sample chamber was first evacuated and then filled with a few mbars of helium as exchange gas. Each spectrum consisted of 100 000 data points in the frequency range 10–1500 kHz or 35 000 data points in the range 10–500 kHz, following automated sequences of varying temperature at constant magnetic field or varying field at constant temperature. Times allowed for thermal equilibration at each set point before data collection were 1 min when varying temperature in small steps at low temperatures (typically for $T <$ ~25 K), or 10 min at higher temperatures. Based on experience over several years and for many materials, this protocol is suitable for long runs without thermal lag. Spectra were analysed offline using the software package Igor (Wavemetrics), with an asymmetric Lorentzian function used for fitting of selected resonance peaks to give values of f and Δf.

4.1. Elastic and anelastic properties in zero field

Figure 1 contains an illustrative stack of segments of primary RUS spectra collected during a heating sequence in zero field. Some resonance peaks show steep reductions in frequency, followed by recovery on heating through the temperature interval ~30–100 K. Variations of f^2 and Q^{-1} from fitting of these provide a quantitative measure of the softening and stiffening and are illustrated in figure 2 for a cooling and heating sequence between 1.5 and 300 K. As found in previous studies on samples with different Co contents [21, 29–31, 34, 35, 42], softening of C_{66} occurs with falling temperature towards T_S due to the pseudoproper ferroelastic character of the structural/electronic transition. The pattern of stiffening below T_S has not been previously observed, however, and elastic softening of the same resonances below the normal—superconducting transition is also clearly visible.

In detail, the variations of different resonance modes with temperature are quite diverse, as illustrated in figure 2(a) for some of the lowest frequency resonance modes. The same diversity is also seen at higher frequencies. Resonances which display the steepest softening have a minimum near 69 K and an interval of ~10 K below this where f^2 values remain approximately constant before the onset of stiffening at lower temperatures (figures 2(a) and (c)). These are accompanied by a peak in acoustic loss which has its onset close to T_S, maximum values of Q^{-1} at ~50–55 K and a return to low values by ~20–30 K. The 31 kHz peak (figure 2(b)) is representative of a small number of weakly excited resonances which show softening only over a narrow temperature interval, with a sharp minimum that is within experimental uncertainty of the value of T_S. This frequency shift is accompanied by a steep rise in Q^{-1} through the same narrow temperature interval instead of the peak in loss at lower temperatures. Q^{-1} increases with increasing temperature above T_S for all resonances but more steeply for some than for others.

None of the resonances investigated in detail show anomalies near 60 K that could be correlated with the antiferromagnetic ordering transition. On the other hand, many resonances show a small softening with falling temperature through T_c.

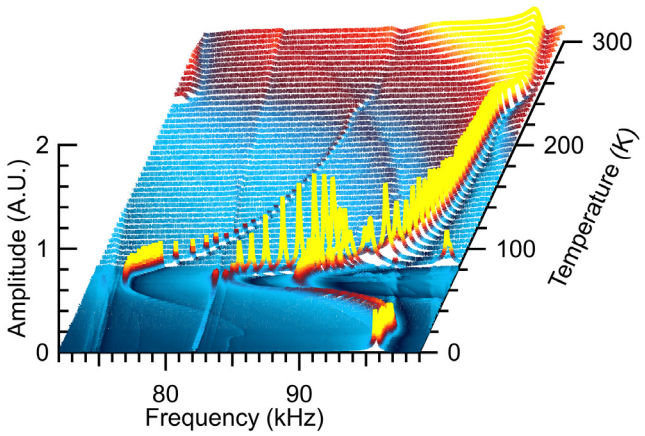

Figure 1. Stack of primary RUS spectra collected during heating in zero field, revealing large variations in frequencies and widths of individual resonance peaks. Each resonance depends on some combination of single crystal elastic constants. Weak resonance peaks showing only slight dependence on temperature in this frequency range are from the sample holder.

All the resonances shown in figure 2 have different values of f^2 between cooling and heating in a single sequence. The change occurred abruptly at ~31 K during cooling and was not repeated in subsequent heating and cooling sequences. This hysteresis is most likely related to some change in the configuration of ferroelastic twins. There is no evidence of hysteretic effects associated with the temperatures at which any of the other elastic anomalies were observed.

The normal—superconducting transition is marked by a slight reduction in frequency of many, but not all, resonance peaks, corresponding to elastic softening of up to ~6%. As shown in figure 3, the amount of softening varied between different resonances, without any associated anomalies in Q^{-1}. The form and magnitude of the changes through T_c were indistinguishable between heating and cooling.

4.2. Elastic and anelastic properties in applied magnetic field

Variations of f^2 and Q^{-1} for selected resonances as a function of temperature through the structural/electronic and magnetic transitions in zero field and in the presence of a 10 T field are compared in figure 4. The sequence of data collection with the field applied was heating from 22 to 150 K, followed by cooling from 150 to 50 K and then heating from 48 to 150 K. There is a small divergence below ~30 K between data collected in zero field and at 10 T, but all the data are close to overlapping between ~40 and ~70 K. There is close correlation of data collected above ~70 K but perhaps with a tendency for values of f^2 measured at 10 T to be slightly lower than those measured in zero field and some slight hysteresis between heating and cooling. While there is evidence for a small influence of field at temperatures above T_S, the 10 T field has little or no effect on the tetragonal–orthorhombic transition.

Figure 5 shows data for f^2 and Q^{-1} measured as a function of increasing and decreasing field up to 9 T at 35, 53, 65, 75 and 85 K. There is a slight increase in f^2 with increasing field

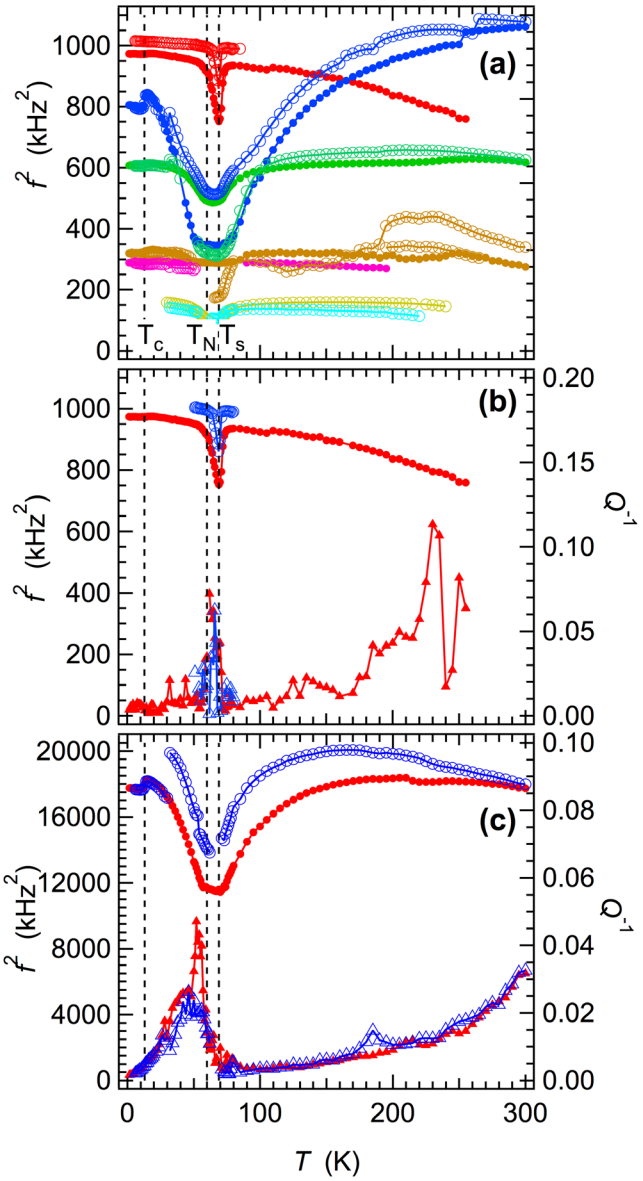

Figure 2. f^2 (circles) and Q^{-1} (triangles) variations for selected resonances in RUS spectra collected during a sequence of cooling (open symbols) followed by heating (filled symbols) in zero magnetic field. Vertical broken lines mark the expected transition temperatures ($T_c = 13$ K, $T_N = 60$ K, $T_S = 69$ K). (a) f^2 variations for resonances at the lowest frequencies show a diversity of patterns of softening/stiffening. (b) One of the weakly excited resonance modes (near 31 kHz at low T) shows steep softening over a narrow temperature interval and a sharp minimum at 69 K, accompanied by high values of Q^{-1} in the same narrow temperature range. Q^{-1} increases more smoothly with increasing temperature above ~100 K though the data become noisy. (c) A resonance mode near 134 kHz at low T, with up to ~36% softening in the temperature interval ~20–150 K, is accompanied by a peak in acoustic loss which has a maximum at ~50–55 K. Marked hysteresis in almost all peak positions appears to arise because of an abrupt change at 31 K during cooling, as seen most clearly for the 134 kHz peak in (c).

at each temperature but Q^{-1} values do not vary. In figure 5(a), which is for the resonance near 31 kHz, the higher values of Q^{-1} at 65 K correspond to the high loss seen at the same temperature in figure 2(b). There is hysteresis below ~3 T at 35 and 53 K, such that the f^2 values are slightly higher with

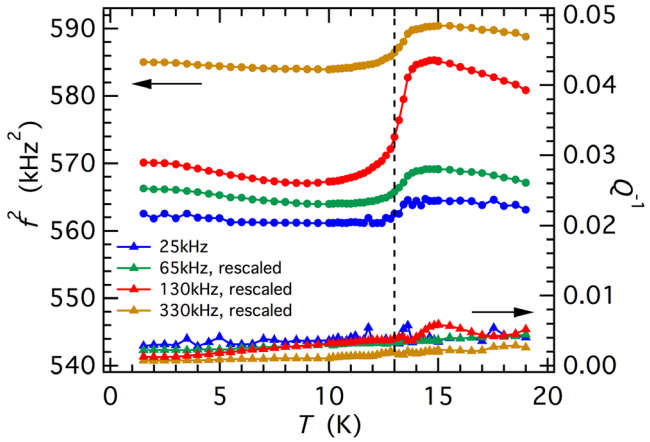

Figure 3. Variations of f^2 and Q^{-1} for resonances that show softening through the normal—superconducting transition (~13 K, vertical dashed line), without any anomalies in Q^{-1}. Values of f^2 for resonances near 63, 131 and 328 kHz have been multiplied by arbitrary scaling factors so that they plot on the same graph. They show the same pattern but with different degrees of softening.

increasing field in comparison with decreasing field, but the differences are close to experimental uncertainty. Figure 5(b) shows data for a resonance with frequency near 32 kHz, which had a similar weak temperature dependence to that shown by the 174 kHz peak in figure 4(c). f^2 values increase slightly and non-linearly with increasing field, with a small hysteresis between increasing and decreasing field below ~3 T at 35 K and below ~5 T at 85 K. Q^{-1} values remain low and constant at all temperatures, though perhaps with a slight increase at the highest fields. Figure 5(c) is a compilation of data from three separate resonances that showed the pattern of marked softening between ~20 and ~150 K seen in figures 2(c) and 4(b). These all show no overt dependence of f^2 or Q^{-1} on field strength. Higher values of Q^{-1} occur at 53 K, corresponding to the high loss seen in the measurements made as a function of temperature at constant field.

The influence of an external magnetic field on the normal—superconducting transition is considered in detail elsewhere [20]. For present purposes it is sufficient to note that the slight softening with falling temperature at low fields becomes marked stiffening at high fields, accompanied by significant anomalies in Q^{-1}.

5. Analysis

5.1. Spontaneous strain, the evolution of Q_E and coupling with Q_M

The *I*4/*mmm*–*Fmmm* transition is accompanied by three non-zero spontaneous strains: e_6 is symmetry breaking while e_1 (=e_2) and e_3 are non-symmetry breaking (appendix equation (A.1)). These are expected to follow the structural/electronic order parameter, Q_E, according to $e_6 \propto Q_E$ and $e_1 \propto e_3 \propto Q_E^2$ due to strain coupling terms of the form $\lambda Q_E e_6$, $\lambda Q_E^2 e_1$, $\lambda Q_E^2 e_3$, where the coefficients, λ, describe the strength of the coupling. Equivalent coupling terms for the antiferromagnetic order parameter, Q_M, have the form $\lambda Q_M^2 e_6$, λQ_M^2

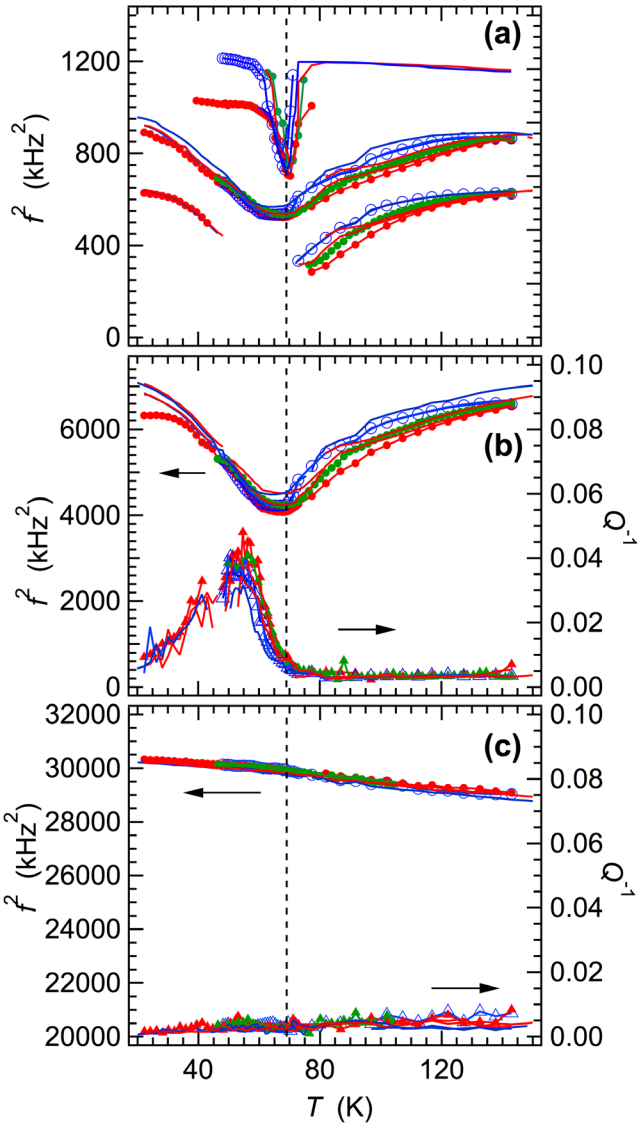

Figure 4. Comparison of f^2 (circles) and Q^{-1} (triangles) variations for selected resonances in RUS spectra collected during successive cooling and heating sequences in zero magnetic field and in a 10 T field ($H//c$). Blue lines = cooling in zero field, red lines = heating in zero field, red symbols = first heat in 10 T field, blue symbols = subsequent cool in 10 T field, green symbols = second heat in 10 T field. Vertical dotted lines are at 69 K. (a) and (b) For resonances which show marked stiffening and softening, there appear to be some systematic differences between zero field and 10 T data below ~30 K, but not in the temperature interval ~40–70 K. The spread between cooling and heating in the temperature interval 80–150 K is slightly larger in the 10 T field than in zero field. All the data for Q^{-1} overlap. (c) A resonance near 174 kHz showing weak temperature dependence has only a slight break in slope in the vicinity of T_S. Application of the 10 T field appears to have no detectable influence on the elastic properties at any temperature.

e_1 and $\lambda Q_M^2 e_3$, so the contributions to e_6, e_1 and e_3 should all scale with Q_M^2. Strain components e_4 and e_5 remain strictly zero.

Figure 6(a) shows variations of e_1 and e_6 calculated from lattice parameter data taken from [6, 48] for samples with $x = 0.045$ and 0.047, respectively (see appendix for details). The maximum values reached are $e_1 \approx -0.0002$ and

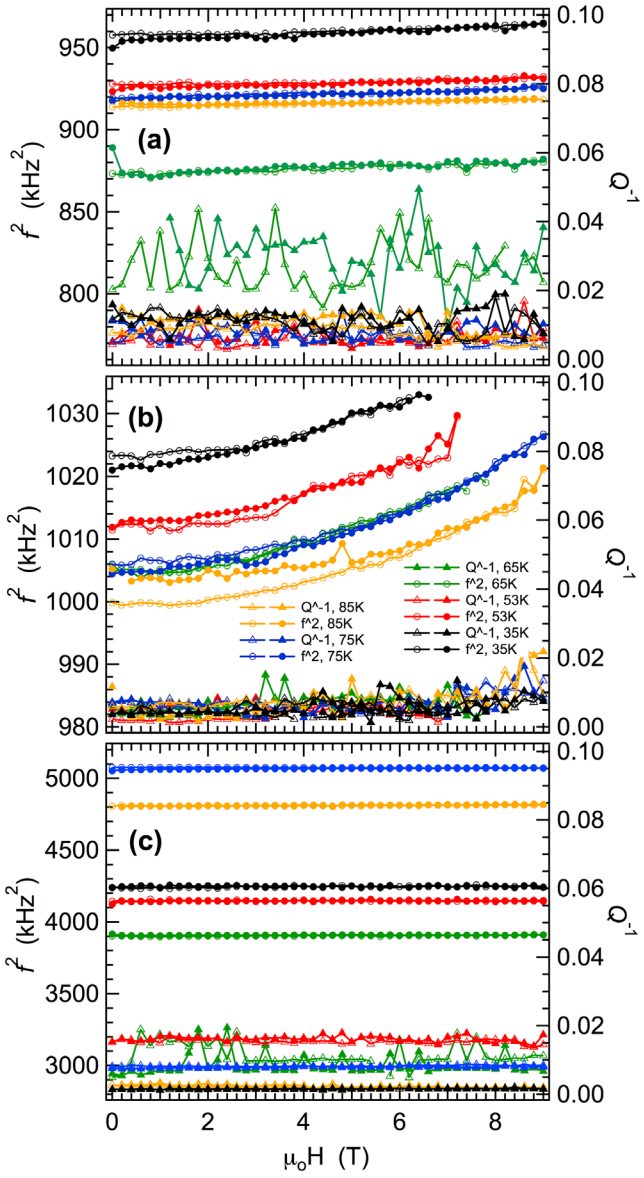

Figure 5. Data for selected resonances collected at 35, 53, 65, 75 and 85 K. Filled symbols represent changes in f^2 (circles) and Q^{-1} (triangles) with increasing field; open symbols show changes during subsequent reducing field. (a) Resonance peak near 31 kHz, for which the temperature dependence is shown in figure 2(b). High values of Q^{-1} at 65 K match up with what is observed in the temperature-dependent data. (b) Resonance peak near 32 kHz, which has the same temperature dependence as shown by the peak near 174 kHz peak in figure 4(c). Hysteresis below ~3 T at 35 K and below ~5 T at 85 K is evident in f^2, with, perhaps, a slight increase in Q^{-1} at the highest fields. (c) Resonances near 65, 85 and 118 kHz, which show the pattern of steep softening between ~20 and ~150 K. f^2 for 85 and 118 kHz resonances were rescaled to allow comparison with the 65 kHz resonance. Relatively high loss at 53 K corresponds to the peak in Q^{-1} seen in measurements made with variable temperature at constant field.

$e_6 \approx 0.003$. Although the compositions of the samples are slightly different, the variations with temperature are clearly consistent with the expected relationship $e_1 \propto e_6^2$. Values of the linear strain e_3 derived from $\Delta c/c$ data for a crystal with $x = 0.038$ of Bud'ko *et al* [58] would be similar in magnitude to e_1 but opposite in sign.

The simplest representation for the evolution of the order parameter at a thermodynamically continuous transition is provided by Landau theory with addition of the saturation temperature, Θ_{so}, (e.g. [59]) as

$$Q^n = A\left[\coth\left(\frac{\Theta_{so}}{T_c}\right) - \coth\left(\frac{\Theta_{so}}{T}\right)\right]. \quad (1)$$

The value of n is 2 for a second order transition and 4 if the transition is tricritical. This has been fit to the data for e_1 ($x = 0.045$) and e_6^2 ($x = 0.047$) in figure 6(a) (both $\propto Q_E^2$), using $n = 2$ and excluding the dip in all strain values below T_c. It is possible also to obtain fits with $n = 4$, but small step-like anomalies in the heat capacity seen in figure A1 (appendix) and reported at T_S for samples with nearby compositions ($x = 0.025$, 0.036, 0.037) [5, 34] confirm that the transition is second order, rather than tricritical, in character.

Figure 6(b) includes data for the intensity of a magnetic ordering reflection from neutron diffraction, $I_{mag} \propto Q_M^2$, (data of [25]) which has been fit in the same way. It shows that the magnetic transition can also be represented as a second order transition, consistent with the small step in heat capacity in figure A1 and as previously reported for a sample with $x = 0.037$ [34]. If there is additional coupling of strains to the magnetic order parameter below T_N it can only be weak as there is no major inflection in the trend of the strain evolution similar to what has been seen in crystals with $x = 0$ or 0.018 [2]. This implies that values of the coupling coefficients λ_{1M}, λ_{4M} and λ_{7M} in equation (A.1) are small at Co-rich compositions. On the other hand, the downturn in e_1 and e_6 below T_c shows that there is some effective strain coupling associated with the order parameter for the normal—superconducting transition.

On the basis of this analysis, the evolution of Q_E below T_S is classically second order in character, and changes in the shear elastic constant C_{66} with temperature for a crystal with $x = 0.043$ are expected to occur through T_S and T_c but not at T_N.

5.2. Evolution of C_{66}, $\frac{1}{2}(C_{11} - C_{12})$ and C_{44}

There are three symmetry-adapted combinations of shear elastic constants to consider with respect to the parent tetragonal structure, $\frac{1}{2}(C_{11} - C_{12})$, C_{66} and C_{44} (appendix table A2, following [32, 34]). Natural acoustic resonances of a small object in an RUS experiment are dominated by shearing motions, typically with only very small contributions from breathing motions. To a reasonable approximation, therefore, the resonance frequencies of most modes will be determined by combinations of these. The orientation of twins in the orthorhombic structure, i.e. sharing a common c-axis, is such that it should still be possible to distinguish between C_{66} and $\frac{1}{2}(C_{11} - C_{12})$. The acoustic resonances determined by C_{44} of the tetragonal structure will be determined by an average of C_{44} and C_{55} of the orthorhombic structure, however.

Because of its irregular shape, the crystal used for RUS could not be used for quantitative determinations of absolute values of the single crystal elastic constants. In order to determine

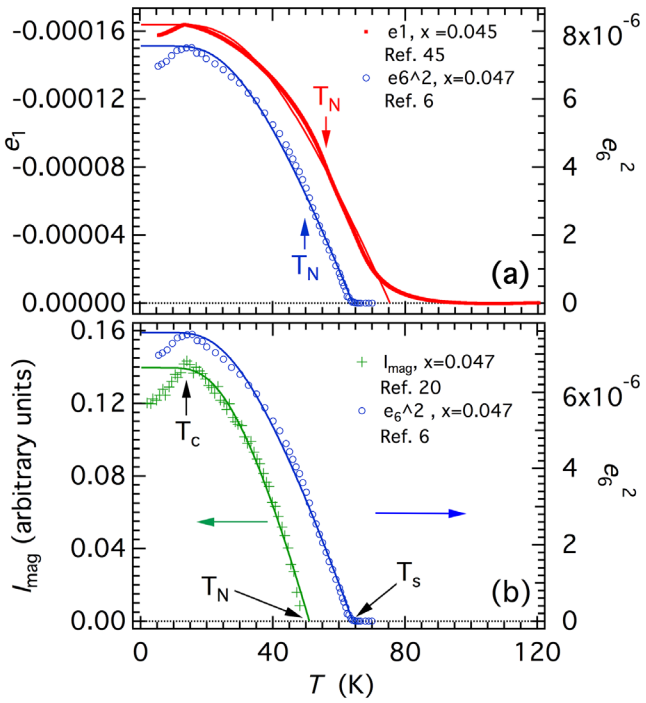

Figure 6. (a) Variation of e_1 determined from the data in figure A5 of the appendix using equation (A.15), and of e_6^2 taken from data of Nandi *et al* [6] using equation (A.14). Solid lines are fits of equation (1): $n = 2$, $A = 2.06 \times 10^{-5}$, Θ_{so} fixed at 60 K, $T_S = 63.7$ K for e_6^2; $A = -0.000\,32$, Θ_{so} fixed at 60 K, $T_S = 75.4$ K for e_1. (b) Variations of the intensity of magnetic ordering reflection, $I_{mag} \propto Q_M^2$, and the square of symmetry breaking shear strain, $e_6^2 \propto Q_E^2$, with fits of equation (1) to represent second order transitions (Θ_{so} fixed at 50 K for I_{mag}), for samples with $x = 0.047$. There may be a small change in trend of e_6^2 at $T = T_N$, but if so, it is very small.

which elastic constants were being expressed by which resonance modes, the rpr program described by Migliori and Sarrao [54] was used instead to calculate resonance frequencies for a tetragonal single crystal having dimensions $0.3 \times 3 \times 4\,\text{mm}^3$, faces parallel to $\{1\,0\,0\}$ and $(0\,0\,1)$, the shortest dimension parallel to $[0\,0\,1]$, and a density of $6.5\,\text{g} \cdot \text{cm}^{-3}$. Data of Simayi *et al* [34], obtained by pulse echo ultrasonics for a crystal with composition $x = 0.037$, were used to provide a set of approximate elastic constants as: $C_{11} = 90$, $C_{33} = 87$, $C_{44} = 38$, $C_{66} = 35$, $C_{12} = 26$, $C_{23} = 23$ GPa ($\frac{1}{2}(C_{11} - C_{12}) = 32$ GPa). An additional approximation was $C_{13} = C_{12}$. The calculation predicts ~15–20 resonance modes below 50 kHz at ~250 K and many more close to T_S where C_{66} becomes much softer. These are shown to be dominated by distortions which depend primarily on $\frac{1}{2}(C_{11} - C_{12})$, C_{66}, or mixtures of the two. C_{44} would be expected to contribute only up to ~15% of selected modes dominated by $\frac{1}{2}(C_{11} - C_{12})$ but hardly at all to those dominated by C_{66}. The influence of $(C_{11} + C_{12})$, C_{33} and C_{13}, presumed to be mainly from breathing motions, is predicted to be small for most resonances.

This result has been used to interpret the temperature dependence of individual resonances in terms of the four different patterns illustrated in figure 7(a). The structural transition is accompanied by classic softening due to a pseudoproper ferroelastic transition, and the resonances labelled as 28 and 378 kHz must be determined predominantly by C_{66}. The 174 kHz resonance shows only a slight temperature dependence and is typical of those of a number seen also at lower frequencies. It must be determined predominantly by $\frac{1}{2}(C_{11} - C_{12})$, consistent with the small temperature dependence seen in pulse-echo ultrasonic measurements ($x = 0.037$) [32, 34, 42]. By far the majority of modes, as represented by the one labelled as 25 kHz in figure 7(a), are then clearly determined by mixtures of $\frac{1}{2}(C_{11} - C_{12})$ and C_{66}.

Resonances which have the largest C_{66} component also show the largest anomaly at T_c, while those dominated by $\frac{1}{2}(C_{11} - C_{12})$ hardly show any influence of the superconducting transition. This leaves a small number of weakly excited modes which have the form shown by the 31 kHz mode. They show a narrow interval of steep softening and a sharp minimum within experimental uncertainty of the value of $T_S = 69$ K. On the basis of the calculated form of modes determined by different combinations of elastic constants, they are presumably due to a combination of $\frac{1}{2}(C_{11} - C_{12})$ with C_{44} or with breathing modes. The contributions of breathing modes are predicted to be even smaller than the contributions of C_{44} and the softening is accompanied by a steep increase in acoustic loss (figure 2(b)) implying that that the changes are anelastic in origin. The softening is therefore tentatively attributed to strong attenuation near T_S of modes which involve the shear strain e_4.

Figure 7(c) reveals the correlation of the magnitude of softening through T_c (13 K) with the magnitude of softening through T_S (69 K). The largest degree of softening observed for any resonance, ~6%, is shown by the one near 28 kHz and is thus associated with C_{66}. There is no overt influence on the resonances near 31 and 174 kHz, which is interpreted as implying that C_{44} and $\frac{1}{2}(C_{11} - C_{12})$ are not affected by the normal—superconducting transition.

5.3. Calibration of the ferroelastic transition

A Landau expansion for the combined ferroelastic transition and magnetic transitions, including the lowest order strain coupling terms, is reproduced in the appendix (equation (A.1)). As discussed in section 5.1, above, e_6 for the ferroelastic phase transition conforms to the pattern expected for a second order transition without coupling to the magnetic order parameter. Leaving out coupling with e_1 and e_3, which is also weak, leads to the simplest form of standard solutions for C_{66} given in the appendix as equations (A.6) and (A.7).

As with previous analyses of the softening of C_{66} as $T \rightarrow T_S$ from above [21, 30, 32, 35, 42], it is necessary to fit the parameters, C_{66}^o, T_{cE}^* and T_{cE}, where C_{66}^o is the elastic constant of the tetragonal structure without any influence of the phase transition, T_{cE} is the critical temperature and T_{cE}^* is the transition temperature renormalized by the bilinear coupling term $\lambda Q_E e_6$. Equation (A.6) has been fit to data for f^2 of the 28 kHz resonance in the temperature interval 80–300 K, the only constraint being that C_{66}^o was set to vary linearly with temperature. The slope was fixed to be that of the Young's

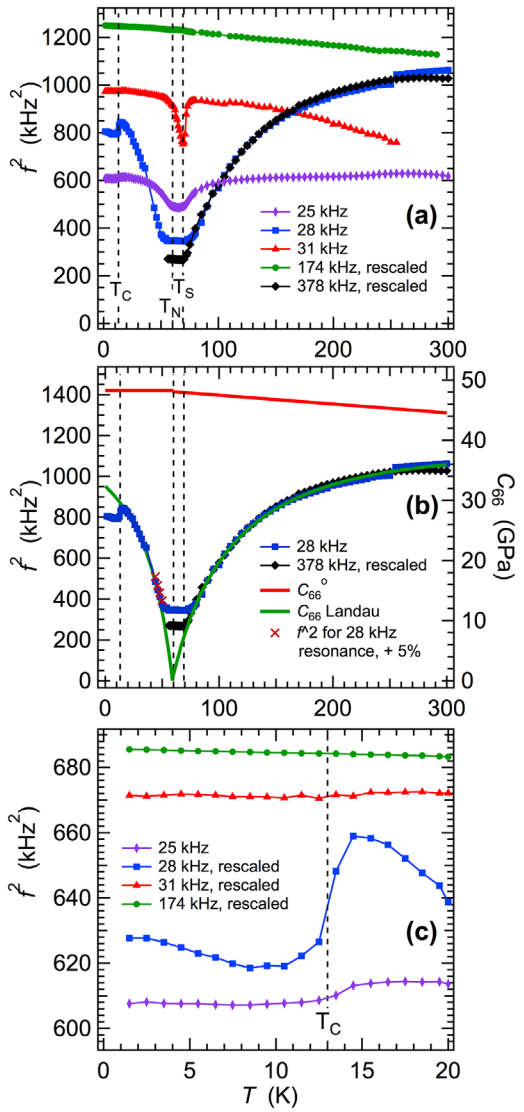

Figure 7. f^2 variations of representative resonance modes in RUS spectra collected during a heating sequence from 1.5 to 300 K. Each mode is labeled according to its approximate frequency at the lowest temperatures. Some have been multiplied by arbitrary scaling factors so that they can be seen in the same graph. (a) 28 and 174 kHz modes correspond to two limiting cases considered to be representative of the temperature dependence of C_{66} and $\frac{1}{2}(C_{11}-C_{12})$, respectively. The 25 kHz mode can then be understood as representing a combination of contributions from $\frac{1}{2}(C_{11}-C_{12})$ and C_{66}. The 31 kHz mode is interpreted as being determined by a combination primarily of $\frac{1}{2}(C_{11}-C_{12})$ and C_{44}. (b) Comparison of experimental data for 28 and 378 kHz resonances with solutions to equations (A.6) and (A.7). The absolute scale for C_{66} (right axis) has been determined by calibration using $C_{66} = 35$ GPa at 250 K for a crystal with composition $x = 0.037$ from [32]. Red crosses are values of f^2 for the 28 kHz resonance increased by 5% to allow for the effect of anelastic softening. (c) Higher resolution view of changes in f^2 through T_c for the resonance modes shown in (a). The resonance which shows the steepest changes through T_S (28 kHz) also shows the largest amount of softening (~6%) through T_c. Resonances which show the least softening associated with the structural transition appear to show no influence due to the normal—superconducting transition.

modulus, $Y_{[1\,1\,0]}$, for $Ba(Fe_{0.67}Co_{0.33})_2As_2$ from Böhmer and Meingast [21]. This is close to slope shown also by the 174 kHz resonance in figure 7(a) ($x = 0.043$, this study) and by both C_{44} and C_{11}–C_{12} in data sets reported for crystals with composition $x = 0.037$ [32,34] and $x = 0.036$ [42]. The fit of equation (A.6) shown in figure 7(b) has $T^*_{cE} = 59 \pm 1$ K and $T_{cE} = 1 \pm 3$ K. Previously reported values of $T^*_{cE} - T_{cE}$ for $Ba(Fe_{1-x}Co_x)_2As_2$ are ~50–60 K, [31] ~30–40 K [21, 35] and ~20 K [42], reflecting some sensitivity to the choice of values for C^o_{66}.

Scaling of f^2 (left axis) to give C_{66} (right axis) in figure 7(b) was achieved by using the value of $C_{66} = 35$ GPa at 250 K given by Yoshizawa and Simayi [32] for a crystal with $x = 0.037$. Equation (A.7) has then been used to calculate C_{66} in the temperature interval 0–59 K, with the only further assumption that C^o_{66} is effectively constant due to the normal effects of saturation as $T \rightarrow 0$ K. As is evident from figure 7(b), the calculated variation, without further fitting, matches the experimental data almost exactly. An additional refinement would be to introduce a saturation temperature in equation (A.3) so as to give the correct evolution with zero slope at 0 K but this would not change the basic conclusion that the overall pattern of evolution of C_{66} fits a simple pseudoproper ferroelastic model over most of the temperature interval between ~20 and 300 K. The important exceptions are that the transition occurs at $T_S = 69$ K instead of $T^*_{cE} = 59$ K and that f^2 remains approximately constant between ~55 and ~70 K instead of tending to zero. Part of the flat segment depends on the extent to which the resonance modes represent mixtures of C_{66}, C_{44} and C_{11}–C_{12}, but it is still present in the most nearly pure C_{66} mode (378 kHz, figure 7(b)).

Determination of parameters from the fitting process allows some of the other Landau coefficients also to be found. From figure 3 of Nandi *et al* [6] a value of $\delta \approx 0.0016$ would be expected for a crystal with composition $x = 0.043$ at 0 K ($\delta \approx e_6/2$). Equation (A.4) then gives $\lambda_{3E} = -0.15$ GPa, assuming $Q_E = 1$ and $C^o_{66} = 48$ GPa. Equation (A.5) gives $a = 0.5$ J · mole^{-1} · K^{-1} based on the calibration 1 GPa $= 6.17 \times 10^4$ J · mole^{-1} · K^{-1} from a molar volume of 6.15×10^{-5} m^3.mole^{-1} for $BaFe_2As_2$, using the unit cell volume of 205 Å^3 given by Huang *et al* [60]. Experimental values for the a coefficient are given separately by the magnitude of the step in heat capacity, ΔC_p, at the transition temperature for a second order transition ($\Delta C_p = a/2$). On this basis, the value predicted from the model is indistinguishable from the observed value $\Delta C_p \approx 0.25$ J · mole^{-1} · K^{-1} (figure A1). By way of comparison, the heat capacity data of Chu *et al* [5] and Simayi *et al* [34] give $a \approx 1.6$, 1.8, 1.5 J · mole^{-1} · K^{-1} at $x = 0.037$, 0.036, 0.025, respectively. Finally, assuming $T^*_{cE} = b/a$, gives $b = 30$ J · mole^{-1}.

From equation (A.1), the expectation is that C_{44} and (C_{11}–C_{12}) will vary according to

$$C_{44} = C^o_{44} + 2\lambda_{6E}Q^2_E + 2\lambda_{5M}Q^2_M \qquad (2)$$

$$\frac{1}{2}(C_{11} - C_{12}) = \frac{1}{2}(C^o_{11} - C^o_{12}) + 2\lambda_{4E}Q^2_E + 2\lambda_{3M}Q^2_M, \qquad (3)$$

where the coupling coefficients can be positive or negative. Data for the 174 kHz resonance are reproduced in figure 8, together with a baseline fit to data in the temperature interval 78–290 K. This shows that there is a small increase below T_S in what is suggested to represent (C_{11}–C_{12}). Both C_{44} and $\frac{1}{2}(C_{11} - C_{12})$ have the same form of anomaly in the data shown by Yoshizawa and Simayi [32] and Kurihara *et al* [42].

5.4. Minor additional influences on the elastic properties

Of much less significance, but included here for completeness, are minor changes in bulk elastic properties arising from additional coupling terms. Firstly, the coupling term $\lambda_{5E}Q_E e_4 e_5$ leads to $C_{45} = \lambda_{5E}Q_E$ for the orthorhombic structure in the setting represented by equation (A.1). In the conventional setting of an orthorhombic crystal, with x- and y-axes rotated through 45°, this term will contribute to C_{44} and C_{55}, causing them to have different values. Its magnitude is not known but the lack of any large anomalies in resonance frequencies relating to combinations of elastic constants other than those which include C_{66} suggests that λ_{5E} is small. Secondly, C_{11} and C_{33} should show the classic stepwise softening arising from coupling terms of the form $\lambda e Q^2$, but these anomalies may not be seen in RUS data which are determined primarily by shearing. Small anomalies with the expected form occur in C_{33} at T_S and T_N in the pulse-echo ultrasonic data for a crystal with $x = 0.037$ [32,34], demonstrating the development of small e_3 strains coupled to both the structural/electronic and magnetic order parameters. A single anomaly in C_{33} occurs in $BaFe_2As_2$, presumably because T_S and T_N are separated by less than ~1 K [1,2] and the two contributions overlap. An equivalent step-like softening has not been seen in ultrasonic data for C_{11} [32,34,42], implying that the coupling of e_1 to any of the order parameters is very weak.

An orthorhombic crystal containing a sufficiently large number of transformation twins due to the symmetry reduction from a homogeneous tetragonal state can still have tetragonal symmetry on a macroscopic scale if there are equal proportions of all possible twin orientations. If the numbers of twins in each orientation is relatively small or there are other features, such as preferential nucleation at the crystal surface, the proportions of different orientations might become unequal. Acoustic resonance frequencies will then depend on the precise distribution of twin walls in the crystal, as has been seen in the case of $LaAlO_3$ where cycling through the ferroelastic transition gives spectra from the low symmetry phase which have slight differences between cycles [61]. Changes in twin configurations during thermal cycling or abruptly at seemingly random temperatures, such as at ~31 K in the cooling sequence shown in figure 2(c), are likely also to have been responsible for some of the changes in resonance frequencies observed in the present study. Hysteresis effects in the configurations of twin lamellae have been observed directly by Tanatar *et al* [62] in AFe_2As_2 (A = Ca, Sr, Ba). The overall pattern of softening and stiffening does not change, however, and the Landau description provides a good representation of the evolution of C_{66} for the orthorhombic phase in spite of the presence of ferroelastic twins, as was found also for C_{44} in twinned rhombohedral crystals of $LaAlO_3$ [63].

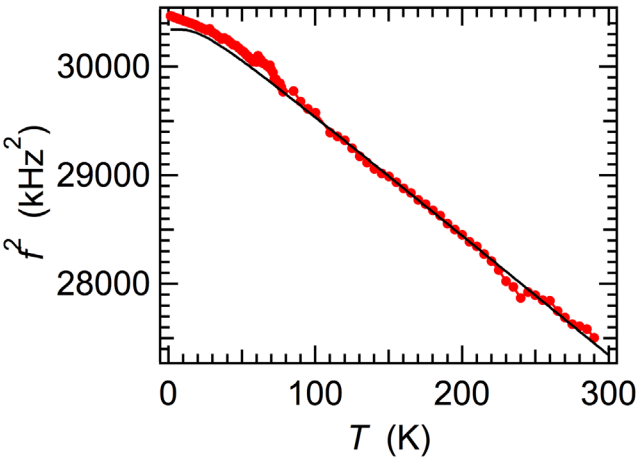

Figure 8. Variation of f^2 for the resonance near 174 kHz. A baseline with the form $f^2 = a_1 + a_2\Theta_s \coth(\Theta_s/T)$ fit to data between 78 and 290 K with $a_1 = 30\,673$, $a_2 = -331.97$ and Θ_s fixed at 30 K, reveals a small increase in the shear elastic constant, suggested to be $\frac{1}{2}(C_{11} - C_{12})$, below T_S.

5.5. Acoustic loss due to thermally activated twin wall motion

The pattern of acoustic loss below T_S resembles the classic Debye-like behaviour associated with freezing processes seen in improper ferroelastic perovskites [43, 61]. Twin walls are expected to be thick and highly mobile immediately below T_S but become thinner with falling temperature. They will be subject to viscous drag due to interaction with defects until they become pinned or frozen below a temperature, T_m, at which $\omega\tau = 1$, where τ is the relaxation time of the twin and ω (=$2\pi f$) is the angular frequency of an applied stress. Typical thermally activated processes responsible for pinning of twin wall motion are expected to follow $\tau = \tau_o \exp(E_a/RT)$, where τ_o is constant, E_a is an activation energy and R is the gas constant. When measured as a function of temperature rather than frequency, the Debye peak in Q^{-1} can be represented by [64, 65]

$$Q^{-1}(T) = Q_m^{-1}\left[\cosh\left\{\frac{E_a}{Rr_2(\beta)}\left(\frac{1}{T} - \frac{1}{T_m}\right)\right\}\right]^{-1}. \quad (4)$$

The maximum value of Q^{-1}, Q_m^{-1}, occurs at temperature T_m and the temperature dependence is determined by the activation energy combined with a spread of relaxation times described by the term $r_2(\beta)$, which represents a Gaussian distribution of relaxation times and equals 1 if there is only a single relaxation time [64, 65].

Figure 9 shows fits of equation (4) to Q^{-1} variations for resonances with frequencies near 80, 90 and 150 kHz. Values of E_a/R from these are 400–750 K (E_a ~ 3–6 kJ · mole^{-1}, ~0.03–0.06 eV), and values of τ_o are on the order of 10^{-9}–10^{-12} s, assuming a single discrete relaxation time ($r_2(\beta) = 1$). Fitting with a single peak reproduces either the width of the loss data but not their shape (figure 9(c)), or part of the shape but not the width (figures 9(a) and (b)), and the existence of

more than one pinning mechanism is implied. Larger values of $r_2(\beta)$, corresponding to some spread of relaxation times, would lead to higher values for E_a/R but these would still be low in comparison with what is expected for a pinning process that involves vacant anion sites.

The activation energy associated with pinning of twin walls by oxygen vacancies [66, 67] in improper ferroelastic oxide perovskites, is ~1 eV ($E_a/R \approx 12\,000$ K). E_a is ~0.15–0.4 eV ($E_a/R \approx 1700$–4600 K) for pinning of twin walls in $KMnF_3$, which has been attributed to the influence of fluorine vacancies [68–70]. Lower values observed here are more likely to be indicative of a dependence of the twin wall mobility on polaronic defects. These have activation energies of ~0.05 eV, as has been proposed for a freezing process of the incommensurate charge ordered structure of $Pr_{0.48}Ca_{0.52}MnO_3$ [71] and an anelastic loss peak in $YBa_2Cu_3O_{6+x}$ [72]. A similar activation energy was found for pinning effects associated with the helical magnetic structure of Cu_2OSeO_3 [57]. The existence of electronic polarons has been predicted in pnictides due to the polarisability of As anions [73], and the activation energy (E_a/R) for polaron-like conduction in $BaFe_2As_2$ has been reported as ~200 K [22].

A purely Debye relationship should also give $Q^{-1} = \Delta\left(\omega\tau/\left(1+\omega^2\tau^2\right)\right)$ where, in the case of a standard linear solid, Δ depends on the difference between the elastic modulus of the relaxed state, C_R, and the unrelaxed state, C_U, according to $\Delta = (C_U - C_R)/C_R$ for $(C_U - C_R) \ll C_R$ [74]. This gives $\Delta = 2Q_m^{-1} \sim 0.05$, representing an anelastic contribution to the change in elastic constants of ~5% for the resonances in figure 2(c). Values of f^2 for the 28 kHz resonance increased by 5% to represent C_U have been added to figure 7(b) (red crosses) in the interval where the measured values represent C_R. They show that the difference is not large enough to affect the conclusion that the Landau description provides a good representation of C_{66} below ~55 K.

5.6. Elastic relaxations associated with antiferromagnetism

The pattern of changes in elastic and anelastic properties expected at a purely antiferromagnetic transition is most clearly illustrated by the reference phase CoF_2. RUS measurements revealed a small degree of precursor softening above T_N, slight softening below T_N consistent with weak coupling of the magnetic order parameter with strain ($\lambda e_i Q_M^2$), an approximately tricritical evolution for the magnetic order parameter and an asymmetric peak in Q^{-1} at T_N [75]. Although a weak loss peak might be obscured by attenuation due to the twin walls, none of these features have been seen near 60 K in the data presented here. The simplest conclusion is again that the magnetic order parameter can only be very weakly coupled with strain in $Ba(Fe_{0.957}Co_{0.043})_2As_2$. Kurihara *et al* [42] reported a break in slope of the temperature dependence of C_{66} at 39 K which was interpreted as being the Néel point of a crystal with $x = 0.036$ but, on the basis of the phase diagram reported by Nandi *et al* [6], the reported values of $T_S = 65$ K and $T_C = 16.4$ K would be more consistent with $x \approx 0.047$. If this revised composition is correct, the expected value of T_N would be ~50 K, rather than 39 K where the anomaly in C_{66} was observed.

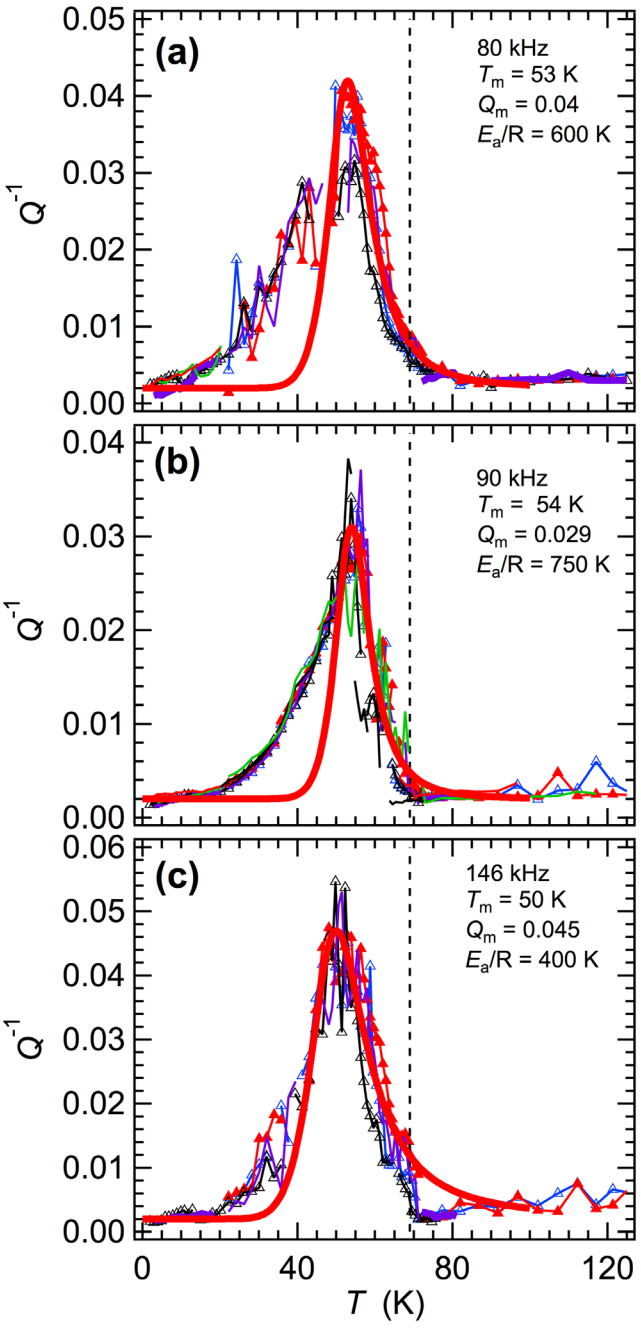

Figure 9. Fits of equation (4) (thick red lines) to data for Q^{-1} from selected resonances (including some data from figure 4(b)), using a baseline of 0.002 and $r_2(\beta) = 1$. The broken vertical line is at $T_S = 69$ K. Given that no single Debye peak provides a good representation of all the data for an individual resonance, it appears that two or more loss peaks are needed to represent the complete behaviour. (a) Resonance peak near 80 kHz. (b) Resonance peak near 90 kHz. (c) Resonance peak near 146 kHz.

A small anomaly in linear thermal expansion has been observed within the *ab* plane of a crystal from the same batch as the present sample [20] and of a crystal with $x = 0.045$ [48]. There appears to be a similarly small effect parallel to the crystallographic *c*-axis in a sample with $x = 0.055$ [48]. These would be expected to give rise to weak step-like

softening of C_{11} and C_{33} during cooling through T_N. As noted in section 5.4, above, softening of C_{33} by up to ~1% has been seen in pulse-echo ultrasonic data from crystals with composition $x = 0.037$ [32,34] or x specified as 0.036 [42] but no equivalent anomaly has been seen in C_{11}. Such small effects would not necessarily be observed in measurements of individual resonance modes in an RUS experiment because of their dependence primarily on shear elastic constants.

Finally, the pulse-echo ultrasonic data showed only minimal changes in C_{44} and $\frac{1}{2}(C_{11} - C_{12})$ through T_N, and this is consistent with the RUS data presented here, confirming that the coupling coefficients in terms $\lambda(e_1 - e_2)^2 Q_M^2$ and $\lambda e_4^2 Q_M^2$ are negligibly small.

5.7. Elastic relaxations associated with the normal—superconducting transition

The pattern of softening of shear elastic constants by a constant amount of up to a few % observed below T_c (figure 3) is essentially what would be expected for a second order transition with a strain, e, weakly coupled to the driving order parameter as $\lambda e Q^2$. The influence is seen most clearly in resonances which are dominated by C_{66}, implying that the coupling of Q_{SC}^2 is with e_6. This is confirmed by the ultrasonic data of Kurihara *et al* [42] which show the same anomaly only in C_{66}. With respect to the tetragonal parent structure, the coupling would be $\lambda e_6^2 Q_{SC}^2$ and, for compositions in the range $x = 0.06$–0.10 where crystals are tetragonal instead of orthorhombic, the pattern for C_{66} is of stiffening rather than softening below T_c (pulse echo ultrasonic measurements at tens to hundreds of MHz [30–32,42], static load three point bending [21] and RUS [24]).

With respect to the orthorhombic structure, when the symmetry is already broken, the coupling would be $\lambda e_{6,SC} Q_{SC}^2$ where $e_{6,SC}$ is the change in e_6 due to the normal—superconducting transition. The fact that $e_{6,SC}$ has opposite sign to e_6 can be understood in terms of the unfavourable coupling of Q_{SC} with Q_E implied by the partial suppression of Q_E below T_c in orthorhombic crystals (figure 6). Changes in other spontaneous strains are negligibly small in comparison with changes in e_6 and, as shown in appendix section A.7, the softening of C_{66} below T_c is then consistent with a simple Landau description (equation (A.13)).

The contribution of twin walls below T_c is revealed by comparison of the evolution of C_{66} with the evolution of Young's modulus, Y_{110}, from static load three point bending measurements on samples with $x = 0.043$ and 0.05. Y_{110} depends on C_{66}, C_{11}, C_{12}, C_{13} and C_{33} (equation (9) of [21]) and a stepwise softening due to strain coupling would be expected. Instead, increases of up to ~0.4% were observed [21]. RUS results for Q^{-1} indicate that the motion of ferroelastic twin walls becomes effectively frozen at temperatures below ~50 K when a small shear stress is applied on a time scale shorter than ~10^{-5}–10^{-6} s. However, if they move in response to the much larger stress of static loading conditions, as seems to be the case [21], the amount of effective softening their motion produces depends on the magnitude of the strain contrast across each wall (super-elastic strain [66]) and, hence, on the magnitude of e_6. Below T_S the e_6 strain increases so that the amount of softening additional to the change in the intrinsic value of C_{66} will increase, giving the net softening with falling temperature reported by Böhmer and Meingast [21]. Below T_c, the magnitude of e_6 decreases due to the unfavourable coupling between Q_{SC} and Q_E, and the trend of slight softening changes to a trend of slight stiffening with further reducing temperature. The reverse of trend of Y_{110} below T_c can therefore be understood as being due to unpinning of the twin walls under relatively high stress and the reverse of the trend of e_6.

The absence of any anomaly in Q^{-1} associated with the normal—superconducting transition contrasts with pulse-echo ultrasonic results from Kurihara *et al* [42] which show a small peak in attenuation at T_c. This indicates critical slowing down of some motion coupled with strain on a time scale of ~10^{-9} s, with dispersion such that it is not detectable on the RUS time scale of ~10^{-5}–10^{-6} s.

6. Discussion

6.1. $T_S \neq T_{cE}^*$, $T_N \approx T_{cE}^*$

From the perspectives of strain and elasticity set out here, the *I*4/*mmm*–*Fmmm* transition in $Ba(Fe_{0.957}Co_{0.043})_2As_2$ conforms quantitatively to a classical mean field model with one order parameter. This applies not only to the softening of C_{66} with falling temperature ahead of T_S [21, 29–35, 42], but also to recovery in the stability field of the orthorhombic structure (figure 7(b)). Such a straightforward treatment does not capture the full physics, however, because the critical shear elastic constant, C_{66}, does not go to zero as $T \rightarrow T_{cE}^*$ in the manner shown by C_{55} at the *Pncm*–$P2_1/c$ transition in LaP_5O_{14} [76], for example. Instead, as noted by Böhmer and Meingast [21], the ferroelastic transition in $Ba(Fe_{1-x}Co_x)_2As_2$ occurs before C_{66} reaches zero. Attempts to fit the data with the constraint $T_S = T_{cE}^*$ did not produce a satisfactory match between calculated and observed variations of C_{66} either above or below T_S, so that the difference $(T_S - T_{cE}^*) \approx 10$ K appears to be robust. Similarly, the value of T_{cE}^* extracted from fitting equation (A.6) to f^2 data in figure 7(b) is sensitive to the choice of baseline to represent to C_{66}^o, but 59 ± 1 K is the same as the value of T_N (60 K) within experimental uncertainty.

Possible explanations of these very particular relationships between T_N, T_S and T_{cE}^* relate to coupling of the structural/electronic ordering parameter with the antiferromagnetic order parameter, the contributions of fluctuations or strain gradient effects and the development of a stabilised ferroelastic microstructure.

6.2. Order parameter coupling

It is well understood that the magnetic and structural/electronic transitions in pnictides have a closely related origin in spin and orbital ordering at the iron atoms ([21, 28, 77, 78] and many references therein), and that magnetoelastic effects are important in these materials (e.g. [6, 23, 77, 79–81]). The

observation of $T_{cE}^{*} \approx T_N$ is a further confirmation, if one were needed, that the magnetic and structural/electronic transitions are intimately related. However, Q_E cannot simply be a secondary order parameter of Q_M (or vice versa), because the structural/electronic and magnetic transitions are observed at two discrete temperatures. This requires that the two order parameters can evolve separately, even though they have closely similar critical temperatures. The lowest order coupling between them permitted by symmetry is linear-quadratic, $\lambda Q_M^2 Q_E$, and this can occur either directly or indirectly by coupling of each order parameter with e_6.

Generic treatments of linear-quadratic coupling [23,82] show that, for the situation equivalent to $T_{cE}^{*} > T_{cM}$, the structural/electronic and magnetic transitions will remain separate. (A single transition would be expected for $T_{cE}^{*} < T_{cM}$). Evidence from the evolution of spontaneous strains and the intensity of magnetic ordering reflections in crystals of $Ba(Fe_{1-x}Co_x)_2As_2$ with $x = 0.045$ and 0.047 (figure 6) is that this coupling must be weak or absent. The lack of any obvious anomaly in C_{66} associated with the antiferromagnetic transition in a crystal with $x = 0.043$ demonstrates more directly that, while coupling of Q_E with e_6 is strong, coupling of Q_M with e_6 is negligible.

The linear-quadratic solution developed by Böhmer and Meingast [31] leads to a different form of evolution of C_{66} (figure 3 of [21]) from what has been observed here for the orthorhombic phase, and the most straightforward conclusion is again that the coefficient for $\lambda Q_M^2 Q_E$ coupling is negligibly small. Anomalies in linear thermal expansion at T_S and T_N in the high resolution data of Meingast *et al* [47] and Bud'ko *et al* [58] for compositions near $x = 0.04$ show that Q_E and Q_M both couple with e_1 and e_3, however, and this must lead to some biquadratic coupling between the two order parameters of the form $\lambda Q_M^2 Q_E^2$. The small magnitude of the observed linear strains ($\lesssim$~0.001) suggests that the coupling would be weak. Generic solutions of Salje and Devarajan [83] for biquadratic coupling show that a sequence of two discrete second order transitions is allowed under this circumstance.

6.3. Fluctuations

Order parameter fluctuations can, in principle, add significantly to the energetics of phase transitions in the vicinity of the transition point. In the context of strain and elasticity, evidence for fluctuations would be precursor softening. In the case of improper ferroelastic transitions in perovskites such as $SrTiO_3$ [84], $LaAlO_3$ [61] and $KMnF_3$ [70], for example, which have a transition driven by a soft optic mode, dynamical softening effects extend to ~15–50 K above the transition temperature. Precursor softening intervals due to dynamic polar nano regions can exceed 100 K if the transition is ferroelectric or relaxor ferroelectric, such as in $BaTiO_3$, $PbSc_{0.5}Ta_{0.5}O_3$ and $PbMg_{1/3}Nb_{2/3}O_3$ [85–87]. No equivalent softening has been seen here in C_{44} and $(C_{11}–C_{12})$ through more than a few degrees above T_S (figure 4), or in any of the individual elastic constants reported by Yoshizawa and Simayi [32], Goto *et al* [30] or Kurihara *et al* [42].

The steep softening shown by resonances such as the one at ~31 kHz between ~57 and ~78 K (figure 2(b)) is accompanied by a steep increase in acoustic loss, which is more indicative of critical slowing down as $T \rightarrow T_S$. There is no independent evidence for the underlying cause but some dynamic aspect of the structure has strain coupling on a timescale of ~10^{-5}–10^{-6} s in the close vicinity of T_S. If the assignment of C_{44} is correct, the strain component is e_4, rather than the symmetry breaking strain, e_6. It is not clear how this would give rise to a difference between T_{cE}^{*} and T_S, and the cause may be related in some way to the early development of a ferroelastic microstructure, as discussed below.

6.4. Local strain gradients

Possible effects of inhomogeneities in a crystal are also not accounted for by the standard Landau expansion used here. Evidence for a locally heterogeneous landscape in $Ba(Fe_{1-x}Co_x)_2As_2$ is provided by high resolution scanning transmission electron microscope imaging [88] and a spread of spin relaxation rates extracted from ^{75}As NMR measurements [89, 90]. The ~8% difference in ionic radii of Co^{2+} and Fe^{2+} in tetrahedral coordination [91] must result in static strain heterogeneities on a unit cell length scale in the solid solution. In the perovskite $(La,Pr)AlO_3$ the diameter of effective strain fields around individual dopant atoms in the perovskite is ~15–20 Å [92] and, in silicates, the equivalent length scale is ~5–40 Å [92].

Disordering of cation vacancies in an otherwise ordered structure also generates local strain heterogeneity and, in the case of the octahedral tilting transition in $La_{0.6}Sr_{0.1}TiO_3$, results in suppression of macroscopic shear strain without suppression of the transition itself [93]. Comparison of pure $BaFe_2As_2$ with Co-doped samples shows what appears to be a similar effect. The magnetic and structural/electronic order parameters are clearly coupled [2,94] in $BaFe_2As_2$ but the coupling appears to diminish with Co-doping [2], as would be expected if local strain fields around Co atoms cause an effective reduction of the coefficient for the coupling term $\lambda e_6 Q_M^2$. Reducing this coupling coefficient has the further consequence that renormalization of the fourth order Landau coefficient will be reduced, so contributing to the change from first order character to second order character reported for the magnetic transition with increasing Co content [2]. The magnitude of the changes in magnetic susceptibility at T_N also diminishes substantially with increasing Co-content [8].

While local strain heterogeneities are most likely to be responsible for the suppression of coupling between Q_M and e_6, it is not immediately clear how they would cause a renormalization of the transition temperature from T_{cE}^{*} to T_S unless strain gradients allow coupling with other order parameter gradients to produce a stable modulated structure of some kind.

Local strain effects are likely also to play a role in the magnetic structure becoming incommensurate when the Co-content is ~0.055–0.06 [7,89,95,96].

6.5. A stabilised ferroelastic microstructure?

The most important omission from the Landau expansion used to describe the ferroelastic transition is the influence of twin walls. Coexisting sets of fine scale twins 90° apart occur in orthorhombic $CaFe_2As_2$, $SrFe_2As_2$ and $BaFe_2As_2$ [62, 97]. These turn into a more diffuse tweed-like texture with increasing K content in $(Ba_{1-x}K_x)Fe_2As_2$ [98] and with increasing Co-content in $Ba(Fe_{1-x}Co_x)_2As_2$ [16]. Local distortions on a nm scale seen at room temperature by high resolution transmission electron microscopy have been proposed as being embryonic to tweed [88]. In general, the width, w, and number density, N, of ferroelastic twin walls are expected to increase as $w \propto N \propto (T_c - T)^{-1}$ at a second order transition as the transition temperature, T_c (or T_c^* for the pseudoproper case), is approached from below [38, 99–101]. Their influence on bulk elastic properties will be greatest in a temperature interval immediately below the transition point, where the effective volume they fill is highest and where they remain mobile.

Following Kityk *et al* [102], changes to the elastic properties are best considered with respect to contributions to the elastic compliance, which are additive. Hooke's law for the relationship between stress σ_6 and strain e_6 can be written as $\sigma_6 = C_{66}e_6$ or $e_6 = s_{66}\sigma_6$, where s_{66} is the compliance. In tetragonal and orthorhombic crystals the relationship between the compliance and elastic stiffness is simply $s_{66} = 1/C_{66}$. For $T < T_S$, C_{66} may therefore be written in terms of a sum of compliances as

$$C_{66} = \frac{1}{s_{66}^{o} + \Delta s_{66}^{e/Q} + \Delta s_{66}^{w} + \Delta s_{66}^{wm}}, \qquad (5)$$

where s_{66}^{o} is the compliance of the reference tetragonal structure, $\Delta s_{66}^{e/Q}$ the contribution from the volume of orthorhombic domains due to the effect of strain/order parameter coupling, Δs_{66}^{w} is a contribution from the volume filled by the twin walls and Δs_{66}^{wm} is the contribution which arises from movement of the twin walls on the time scale of the measurements. The sum $s_{66}^{o} + \Delta s_{66}^{e/Q}$ increases due to the intrinsic effect of strain coupling and, theoretically, will become infinite at the critical temperature for a second order transition. Δs_{66}^{w} will always be finite, however, since the twin walls effectively have the structure of the parent tetragonal structure. This is mitigated to some extent by the fact that easy motion of the walls under an externally applied stress will cause their effective contribution, $\Delta s_{66}^{w} + \Delta s_{66}^{wm}$, to increase but, in terms of stiffness, the presence of twin walls will ensure that the value of C_{66} for the bulk material does not go to zero. Instead, there has to be a temperature interval near the transition point where C_{66} is determined predominantly by the relatively stiff but mobile twin walls rather than softening within the domains. This can account for the interval seen in figure 7(b) where f^2 values remain constant.

Twin wall motion is constrained by an effective viscosity due to interactions of strain gradients of the walls with strain fields of defects but ceases once the twin walls become pinned. From the acoustic loss data, the pinning temperature for motion on a time scale of ~10^{-5}–10^{-6} s under conditions of low stress is ~50–55 K (figure 5). This coincides with the upturn of f^2 data representing C_{66} in figure 7(b), consistent with the view that the flat segment is due to the influence of mobile ferroelastic twin walls.

By themselves, the presence of twin walls as defects in otherwise homogeneous crystals would not be responsible for the shift of the expected transition point, given by T_{cE}^*, to the observed transition point, given by T_S. However, if there was any energetic advantage from coupling with strain gradients of more than one order parameter, a stable modulated microstructure might add to the stability of the orthorhombic phase. The question is then whether there is any evidence for a second order parameter which might contribute to the stability of an intermediate state between T_S and T_{cE}^* in $Ba(Fe_{1-x}Co_x)_2As_2$. The most obvious candidate would be the antiferromagnetic order parameter, Q_M, but it is already clear that coupling between Q_M and e_6 is weak and there is no evidence for a separate strain-related phase transition at T_{cE}^*. Furthermore, if magnetic ordering was important, some influence of magnetic field on the elastic properties might be expected in this temperature interval and none is observed (figure 4).

An alternative is suggested by the anomaly in C_{44} (or C_{11}–C_{12} if the assignment given above to the 31 and 174 kHz resonances is the other way round), with the maximum at exactly T_S and the lower limit at $T_N \approx T_{cE}^*$. The anelastic character signifies slowing down of some lattice mode or aspect of the microstructure which is associated with e_4 (or e_1–e_2) and which could be associated with a second order parameter. On this basis, a potentially viable but untested explanation of the difference between T_S and T_{cE}^* would be the existence of a microstructure with unpinned twin walls and some strain gradient coupling which causes additional stabilization of orthorhombic crystals through a temperature interval which extends to ~10 K above T_{cE}^*. Testing of this model might focus on dynamic properties from a central peak effect, such as has been observed in inelastic neutron scattering in a crystal of $BaFe_2As_2$ by Niedzela *et al* [103], and the critical slowing down of C_{44} (or C_{11}–C_{12}).

6.6. Defects and twin wall pinning

A recurring theme in the literature on pnictides is evidence for heterogeneity on a local scale that shows up particularly in the superconducting phase (e.g. [77, 89, 90, 104–107]) and may be due to inhomogeneous strain, chemistry or defect distributions. In the case of $BaFe_2As_2$, an applied magnetic field does not appear to have a direct influence on the electronic/structural transition but the structural and magnetic transitions are sensitive to the effects of annealing at 700 °C [1,4,108]. T_c for the superconducting transition in Co-doped samples is also increased by a few degrees following annealing at 750 °C [109] or 800 °C [108,110]. Variations in elastic properties seen here in repeated measurements through the interval between T_S and room temperature (figure 4) are suggestive of the presence of some array of defects or heterogeneities which are coupled with strain. A spread between heating and

cooling in zero field is essentially the same as for increasing and decreasing field at 85 K (figure 5(b)), implying that the array can be rearranged in tetragonal crystals by a magnetic field as well as by heating up to room temperature. This suggests that they are not simply static strain effects associated with the distribution of Co substituted for Fe.

X-ray linear dichroism experiments at $T > T_S$ reported for $Ba(Fe_{1-x}Co_x)_2As_2$ have revealed a significant signal for local orbital ordering [111], which can also be understood from the perspective of electronic polarons [112]. Polarons or bipolarons with the same local structure as the ordered phases at lower temperatures [22] would be expected to couple with local strains. The temperature of ~140 K from the x-ray data for the onset of local ordering at $x = 0.05$ is ~10–50 K below the temperatures at which there is an increase in conductance with falling temperature [113] and there is a change in the properties of Raman spectra [114]. A feature of the RUS data which may be related to a change of defect dynamics or density at this temperature is the increasing acoustic loss with increasing temperature above ~130–150 K (figures 2(b) and (c)). The same, or related defects are likely to be responsible for pinning of the ferroelastic twin walls.

6.7. Domain wall engineering

A current topic of close interest is the structure and behaviour of domain walls, which can have properties that are quite distinct from the matrix in which they sit and which have potential for new technological advances (e.g. [10, 11, 13]). The most interesting materials in this context are those which have multiple and interacting instabilities because of the possibilities that then occur for coupling between different properties at the twin walls. These issues have been raised in particular for multiferroic domain walls, but in tungsten oxide the twin walls can be superconducting while the matrix has normal conductivity [115]. In pnictides, new combinations of properties relate to magnetism and superconductivity. Structural and orientational relationships between magnetic and ferroelastic domain walls have already been considered and there is experimental evidence both for changes in the superconducting properties at the twin walls and their interaction with vortices [15, 116–119]. In contrast with the behaviour of vortices in YBCO, it appears that the vortices avoid pinning to the twin walls [15]. These effects should all be tunable by choice of chemistry, magnetothermal history and, for thin film applications, by choice of substrate. The important observation here is that strain coupling will be a fundamental factor, including the effects of heterogeneity.

7. Conclusions

The most general conclusion from this comprehensive investigation of elasticity, heat capacity and magnetism is that strain does indeed permeate every aspect of the overall behavior and properties of a Co-doped pnictide, down to the finest details of how elastic and anelastic properties respond to changes in temperature and magnetic field. Although the experimental data relate only to $Ba(Fe_{1-x}Co_x)_2As_2$, the pnictides define a distinct class of multiferroic superconductors with some diversity. In $(Ba_{1-x}K_x)Fe_2As_2$ and $(Ba_{1-x}Na_x)Fe_2As_2$, there is a single transition to an orthorhombic, antiferromagnetic phase but there exist also stability fields for a magnetically ordered tetragonal structure [78, 98, 120, 121]. FeSe has a tetragonal–orthorhombic transition without magnetic ordering [122, 123]. It must be expected that common to all these, and the cause of some of the differences, will be variations in the strength of coupling between strain and individual order parameters. More specifically it has been concluded that:

1. The structural/electronic component of the overall transformation behaviour of $Ba(Fe_{0.957}Co_{0.043})_2As_2$, conforms to the precepts of Landau theory for a pseudoproper ferroelastic transition with second order character. This has been demonstrated through the stability fields of both the tetragonal and orthorhombic structures, with the exception that the transition occurs ~10 K above the temperature at which C_{66} would tend to zero.
2. Coupling of the magnetic order parameter with the shear strain e_6 appears to be negligibly small, most likely due to the influence of local strain heterogeneity associated with substitution of Co for Fe. As a result, the indirect contribution to linear-quadratic coupling between the structural/electronic and magnetic order parameters is negligible. No evidence has been found, either, for direct linear-quadratic coupling. Biquadratic coupling via the non-symmetry breaking strains remains a possibility but the relevant strains are small.
3. Ferroelastic twin walls in the orthorhombic phase are mobile on a timescale of ~10^{-5}–10^{-6} s under the application of a dynamic stress but become immobile below ~55 K due to pinning by defects. The activation energy associated with the pinning process, ~0.05 eV, is tentatively attributed to polaronic defects.
4. The ferroelastic transition is not influenced by a magnetic field up to ~10 T, but acoustic loss and some hysteresis effects in the stability field of the tetragonal phase suggest the existence of magnetoelastic defects which may also be responsible for the pinning process at lower temperatures.
5. The difference between the transition temperature, T_S, and the temperature at which C_{66} extrapolates to zero, T^*_{cE}, is not due overtly to coupling of the structural/electronic order parameter with a second order parameter. One untested possibility is that a ferroelastic microstructure is at first stabilized by coupling between strain gradients.
6. Coupling of the superconducting order parameter with shear strain, e_6, occurs indirectly through unfavourable coupling with the structural/electronic order parameter. The observed strain variations and elastic softening are

consistent with being due to coupling which is effectively of the form $\lambda e_6 Q_{SC}^2$ at a second order phase transition, where e_6 here is the change in shear strain with respect to the orthorhombic structure.

Acknowledgments

RUS facilities in Cambridge were established through grants from the Natural Environment Research Council and the Engineering and Physical Sciences Research Council of Great Britain to MAC.: EP/I036079/1, NE/B505738/1, NE/F17081/1. The work presented here was funded specifically through NE/F17081/1. AC magnetic measurements were carried out using the Advanced Materials Characterisation Suite, funded by EPSRC Strategic Equipment Grant EP/M000524/1. PM acknowledges funding from the Winton Programme for the Physics of Sustainability. Tony Dennis is thanked for help with collecting and analyzing the DC magnetic data.

Appendix

The experimental data and Landau expansions given here have been separated from the main paper because they are supplementary to the substance of the study, which relates to strain relaxation behavior. Unlike in many previous studies of phase transitions in pnictides, however, the measurements were all made on crystals from the same batch so as to allow close correlations to be made of structural, magnetic, thermodynamic and mechanical properties.

A.1. Heat capacity

Crystal 2 was used for heat capacity measurements in a Quantum Design PPMS. The data were collected during heating in 0.1 K steps in external fields of 0, 1, 2.5, 5 and 7.5 T applied parallel to the crystallographic *c*-axis (*H*//*c*). As shown in figure A1, there are small anomalies at ~69 and ~60 K, confirming the structural/electronic and antiferromagnetic transition temperatures. The form of the anomalies is consistent with the small step, ΔC_p, expected at a second order transition, with some smearing over a small temperature interval close to T_N and T_S. Values of ΔC_p at T_N and T_S are ~0.15 and ~0.25 J · mole^{-1} · K^{-1}, respectively. No evidence was found for any significant effect of magnetic field on these transitions between zero field and 7.5 T.

A.2. DC magnetic properties

Measurements of DC magnetic moment were made on Crystal 2 in a Quantum Design MPMS XL squid magnetometer with *H*//*c*. These did not reveal any significant anomaly at the structural or magnetic transition temperatures in heating and

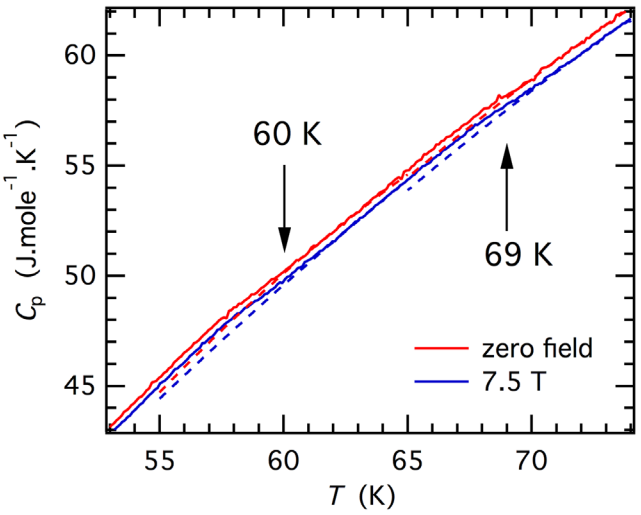

Figure A1. Heat capacity of Crystal 2. Dashed lines are fits to the data in a small temperature interval above the expected transition temperatures, with extrapolations to lower temperature. There are small, stepwise but slightly smeared anomalies at $T_N \approx 60$ K, $T_S \approx 69$ K.

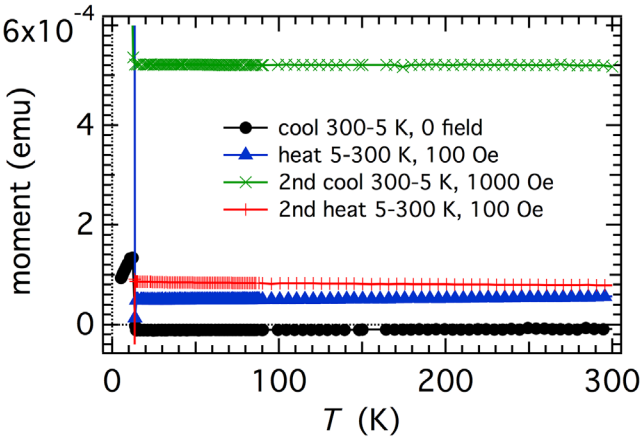

Figure A2. DC moment from two cooling and heating sequences with different fields applied parallel to the crystallographic *c*-axis of crystal 2. The data are plotted as moment rather than moment/field to show that there are no overt changes associated the structural transition (69 K) or the Néel point (60 K) and also that there are no changes associated with changes in configuration of ferroelastic twin walls during repeated cycling in different fields. The superconducting transition is clear from the abrupt changes in moment near 13 K.

cooling sequences with and without applied field (figure A2). The superconducting transition is clearly seen as an abrupt change in moment near 13 K.

Magnetic hysteresis loops (*H*//*c*) were measured to ±67 kOe (6.7 T) at selected temperatures in the MPMS instrument in two cooling sequences. The first sequence was from 300 to 50 K and the second from 15 to 5 K, with removal and reloading of the sample from the instrument between

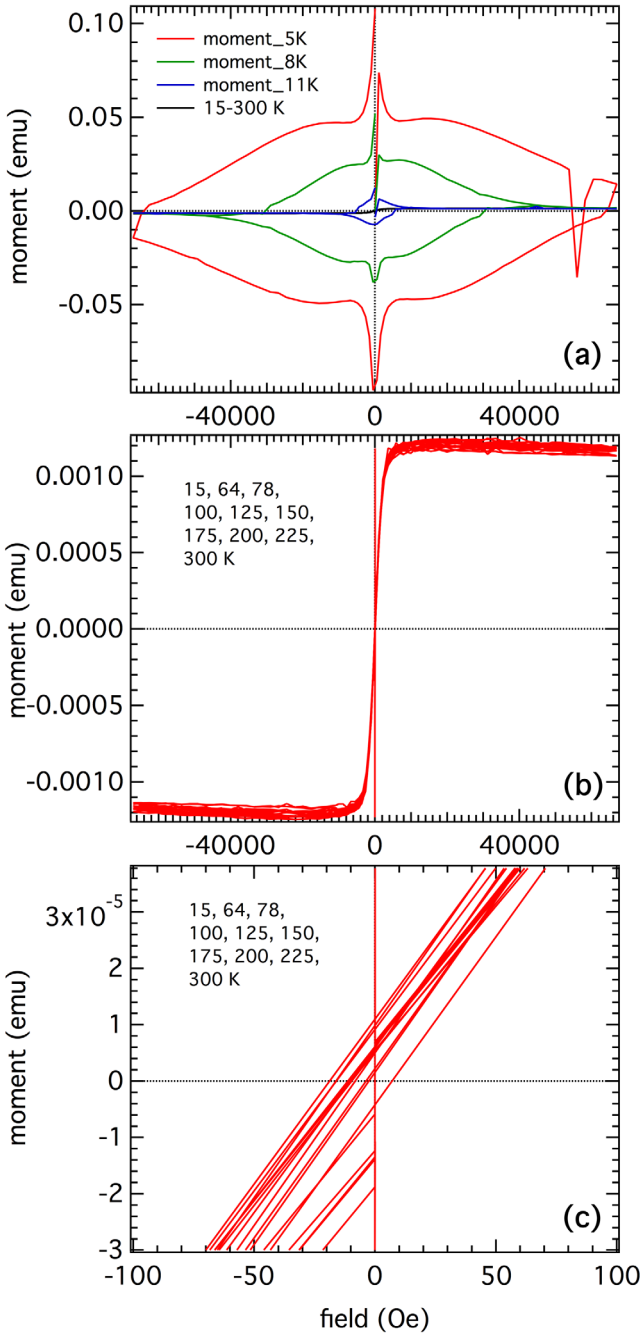

Figure A3. Magnetic hysteresis loops for crystal 2 ($H//c$) from two separate cooling sequences, 300 to 50 K, and then 15 to 5 K. (a) Below T_c the fishtail pattern is characteristic of unconventional superconductivity. (b) Above T_c there is a weakly ferromagnetic component. Individual loops have the pattern of a weakly ferromagnetic component with small opening, but the saturation magnetization is independent of temperature. At large fields the overall weakly negative slope suggests some diamagnetic component; this slope is reversed (paramagnetic) at 50 K. (c) Expanded view of the small openings of loops shown in (b).

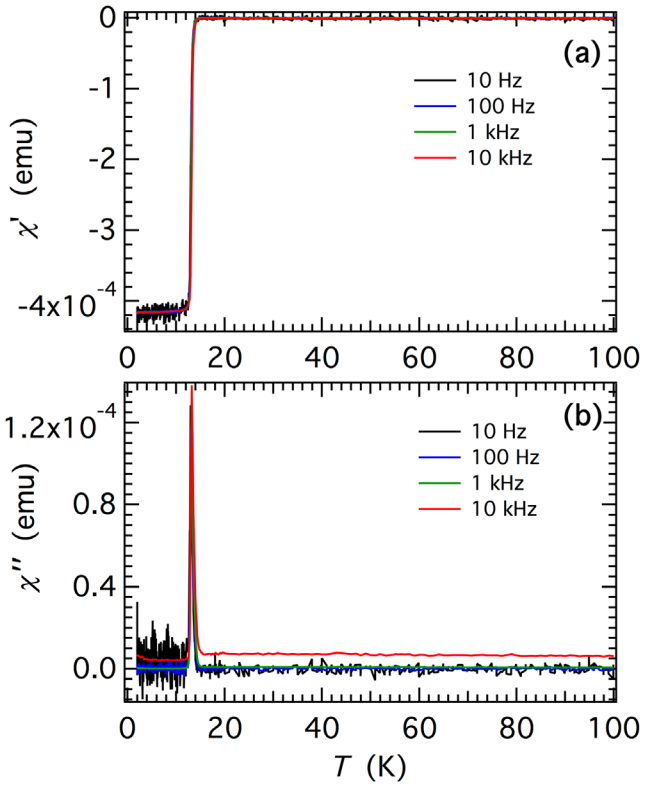

Figure A4. Real (a) and imaginary (b) components of the AC magnetic susceptibility from crystal 2 under a DC field of 20 Oe ($H//c$). The superconducting transition shows up clearly at ~13 K, with a very slight dependence on measuring frequency, but there are no overt magnetic anomalies at higher temperatures.

them. An overview of the data (figure A3(a)) shows the characteristic fishtail pattern for an unconventional superconductor below T_c, and a weakly ferromagnetic component at all temperatures above T_c. Enlarged views of the loops above T_c (figures A3(b) and (c)) show that the saturation magnetization of the ferromagnetic component is independent of field and that the openings are small. Most of the data in figure A3(b) have a weakly negative temperature dependence at high fields, perhaps indicating a diamagnetic component, with only the loop collected at 50 K showing positive (paramagnetic) slope. It is also possible that this change in slope is an artefact, arising from the crystal not being perfectly centered in the instrument. The weak ferromagnetic moments are most likely due to some discrete impurity phase or to local moments associated with Fe atoms, rather than ferromagnetic ordering of the pnictide phase itself.

A.3. AC magnetic properties

Measurements of AC magnetic properties were made on the same crystal using the AC Measurement System option in a

Table A1. Possible subgroup structures derived from *I*4/*mmm* (or *I*4/*mmm*1′) on the basis of non-zero order parameters belonging to irreducible representations Γ_4^+ and mX_2^* (see also [37]). Note that $C_A mca$ is the conventional setting for the orthorhombic structure of $BaFe_2As_2$ which is usually given a setting with lattice vectors (1,1,0)(−1,1,0)(0,0,1) that would be described as $B_A bcm$.

Space group	Γ_4^+	mX_2^*	Allowed to be continuous	Lattice vectors	Origin
*I*4/*mmm* (139)					
*I*4/*mmm*1′ (139.532)	(0)	(0,0)		(1,0,0)(0,1,0)(0,0,1)	(0,0,0)
*Fmmm*1′ (69.522)	(*a*)	(0,0)	Yes	(1,1,0)(−1,1,0)(0,0,1)	(0,0,0)
P_C4/*mbm* (127.397)	(0)	(*a*,*a*)	Yes	(−1,1,0)(−1, − 1,0)(0,0,1)	(−1/2,1/2,0)
$C_A mca$ (64.480)	(*a*)	(0,*b*)	Maybe[a]	(0,0,1)(1,1,0)(−1,1,0)	(0,0,0)
$P_C bam$ (55.363)	(*a*)	(*b*,*c*)	No	(1,−1,0)(1,1,0)(0,0,1)	(0,0,0)

[a] ISOSUBGROUP shows that the transition can be continuous if driven by mX_2^* with Γ_4^+ as a secondary order parameter (i.e. just one active *k*-vector) but not if Γ_4^+ is also imposed (i.e. a second active *k*-vector). In the latter case, there would be a continuous transition to *Fmmm* and then another continuous transition to $C_A mca$.

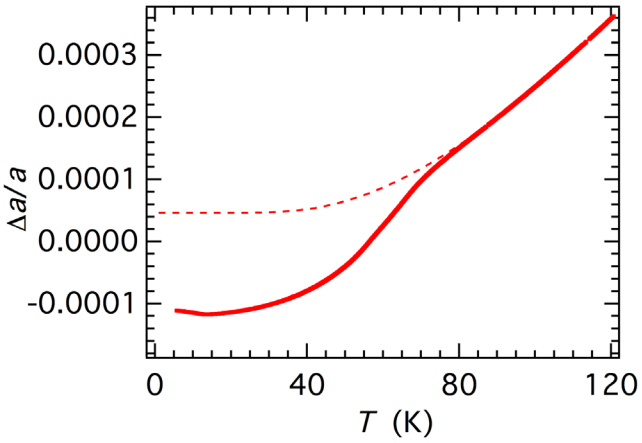

Figure A5. Relative length change of single crystal of $Ba(Fe_{0.955}Co_{0.045})_2As_2$ ([48]) with a fit of equation (3) to the data above T_S (dashed line): $a_1 = -8.37 \times 10^{-4}$, $a_2 = 7.76 \times 10^{-6}$, $\Theta_s = 113.8$ K.

Quantum Design PPMS instrument at frequencies of 0.01, 0.1, 1, 10 kHz, with a DC field of 20 Oe and amplitude 3 Oe for the driving AC field (*H*//*c*). Data were collected during heating in steps of 0.2 K between 2 and 20 K, and of 1 K between 20 and 100 K. Neither the real component, χ', nor the imaginary component, χ'', of the magnetic susceptibility showed any overt magnetic anomalies between ~15 and 100 K (figure A4). The superconducting transition is marked by a steep change in χ' between ~12 and ~15 K (figure A4(a)) and a sharp peak in χ'' through the same interval (figure A4(b)), with a slight frequency dependence.

A.4. Landau theory

The conventional setting of the magnetic space group of the antiferromagnetic orthorhombic structure of $BaFe_2As_2$ is $C_A mca$, and the parent tetragonal structure has space group *I*4/*mmm* (grey group *I*4/*mmm*1′) [36,37]. The transition *I*4/*mmm*1′–$C_A mca$ can be driven by an order parameter with the symmetry of the irreducible representation mX_2^* alone or by a combination of this order parameter with a structural order parameter that transforms as a gamma point irreducible representation, Γ_4^+, of space group *I*4/*mmm*. If it was driven by the mX_2^* order parameter alone, the transition would be improper ferroelastic, whereas a transition *I*4/*mmm*–*Fmmm* driven by the Γ_4^+ order parameter would be pseudoproper ferroelastic. The full range of possibilities which arise from a combination of the two order parameters is listed in table A1, as derived using the group theory program ISOSUBGROUP [124].

Treating the combined structural and magnetic transitions as having two discrete order parameters and separate critical temperatures, a Landau expansion including lowest order strain coupling terms (but not including order parameter saturation) would be, from ISOTROPY [125],

$$
\begin{aligned}
G = {} & \tfrac{1}{2}a_{\mathrm{E}}\left(T - T_{\mathrm{cE}}\right)Q_{\mathrm{E}}^2 + \tfrac{1}{4}b_{\mathrm{E}}Q_{\mathrm{E}}^4 \\
& + \lambda_{1\mathrm{E}}Q_{\mathrm{E}}^2\left(e_1 + e_2\right) + \lambda_{2\mathrm{E}}Q_{\mathrm{E}}^2 e_3 + \lambda_{3\mathrm{E}}Q_{\mathrm{E}}e_6 + \lambda_{4\mathrm{E}}Q_{\mathrm{E}}^2\left(e_1 - e_2\right)^2 + \lambda_{5\mathrm{E}}Q_{\mathrm{E}}e_4e_5 + \lambda_{6\mathrm{E}}Q_{\mathrm{E}}^2\left(e_4^2 + e_5^2\right) \\
& + \tfrac{1}{2}a_{\mathrm{M}}\left(T - T_{\mathrm{cM}}\right)\left(m_1^2 + m_2^2\right) + \tfrac{1}{4}b_{\mathrm{M}}\left(m_1^2 + m_2^2\right)^2 + \tfrac{1}{4}b'_{\mathrm{M}}\left(m_1^4 + m_2^4\right) \\
& + \lambda_{1\mathrm{M}}\left(m_1^2 + m_2^2\right)\left(e_1 + e_2\right) + \lambda_{2\mathrm{M}}\left(m_1^2 + m_2^2\right)e_3 + \lambda_{3\mathrm{M}}\left(m_1^2 + m_2^2\right)\left(e_1 - e_2\right)^2 + \lambda_{4\mathrm{M}}\left(m_1^2 - m_2^2\right)e_6 \\
& + \lambda_{5\mathrm{M}}\left(m_1^2 - m_2^2\right)e_4e_5 + \lambda_{6\mathrm{M}}\left(m_1^2 + m_2^2\right)\left(e_4^2 + e_5^2\right) + \lambda_{7\mathrm{M}}\left(m_1^2 + m_2^2\right)e_6^2 \\
& + \lambda_{1\mathrm{EM}}\left(m_1^2 - m_2^2\right)Q_{\mathrm{E}} + \lambda_{2\mathrm{EM}}\left(m_1^2 + m_2^2\right)Q_{\mathrm{E}}^2 \\
& + \tfrac{1}{4}\left(C_{11}^{\mathrm{o}} + C_{12}^{\mathrm{o}}\right)\left(e_1 + e_2\right)^2 + \tfrac{1}{2}\left(C_{11}^{\mathrm{o}} - C_{12}^{\mathrm{o}}\right)\left(e_1 - e_2\right)^2 + C_{13}^{\mathrm{o}}\left(e_1 + e_2\right)e_3 + \tfrac{1}{2}C_{33}^{\mathrm{o}}e_3^2 + \tfrac{1}{2}C_{44}^{\mathrm{o}}\left(e_4^2 + e_5^2\right) \\
& + \tfrac{1}{2}C_{66}^{\mathrm{o}}e_6^2. \qquad \text{(A.1)}
\end{aligned}
$$

Table A2. Symmetry-adapted elastic constants (eigenvalues) and strains (from the eigenvectors) of the elastic constant matrix for point group 422 (Laue class 4/*mmm*).

Irreducible representation	Eigenvalue	Eigenvector	Symmetry-adapted spontaneous strain
A_1	$\frac{1}{2}\left\{\begin{array}{l}(C_{11}+C_{12}+C_{33})\\ -\left[(C_{11}+C_{12}-C_{33})^2+8C_{13}^2\right]^{1/2}\end{array}\right\}$	$(\alpha,\alpha,\beta,0,0,0)$	$(e_1+e_2)\,;e_3$
A_1	$\frac{1}{2}\left\{\begin{array}{l}(C_{11}+C_{12}+C_{33})\\ +\left[(C_{11}+C_{12}-C_{33})^2+8C_{13}^2\right]^{1/2}\end{array}\right\}$	$(\alpha',\alpha',\beta',0,0,0)$	$(e_1+e_2)\,;e_3$
B_1	C_{11}–C_{12}	$\left(\frac{1}{\sqrt{2}},-\frac{1}{\sqrt{2}},0,0,0,0\right)$	$e_o=\frac{1}{\sqrt{2}}(e_1-e_2)$
B_2	C_{66}	$(0,0,0,0,0,1)$	e_6
E	$\left\{\begin{array}{l}C_{44}\\ C_{44}\end{array}\right.$	$A(0,0,0,1,0,0)$ $B(0,0,0,0,1,0)$	e_4 e_5

Note. $2\alpha^2+\beta^2=2\alpha'^2+\beta'^2=1$, $2\alpha\alpha'+\beta\beta'=0$, $A^2+B^2=1$. A semi-colon is placed between two strains to signify that, although they have the same symmetry, they would develop in different proportions according to the values of the coefficients α, β, α' and β'.

Q_E is the structural order parameter and subscript E signifies all the related Landau coefficients. Individual strains are specified as e_i, $i=1$–6, and C_{ik}^o represents the elastic constants of the reference tetragonal structure. In the C_Amca structure, $m_1=0$, $m_2=Q_M$ and $(m_1^2+m_2^2)$ can be replaced by a single magnetic order parameter, Q_M^2. The subscript M signifies the associated coefficients. Linear-quadratic coupling between the two order parameters can be direct, $\lambda_{1EM}Q_M^2Q_E$, or indirect via the common strain, e_6. Biquadratic coupling is always allowed and can also be direct, $-\lambda_{2EM}Q_M^2Q_E^2$, or indirect via common strains (e_1+e_2), e_3. The transitions *I*4/*mmm*–*Fmmm*–C_A*mca* and *I*4/*mmm*—C_A*mca* are all permitted by symmetry to be second order in character.

In the simplest limiting case, coupling between Q_M and Q_E is weak, Q_M does not couple significantly with e_6 and the non-symmetry breaking strains are negligibly small. The evolution of C_{66} is then determined by the evolution of Q_E and the bilinear coupling with e_6. The description for a second order transition becomes

$$G=\frac{1}{2}a_E\left(T-T_{cE}\right)Q_E^2+\frac{1}{4}b_EQ_E^4+\lambda_{3E}Q_Ee_6+\frac{1}{2}C_{66}^oe_6^2 \quad (A.2)$$

with well known standard solutions (e.g. from [126]), including

$$G=\frac{1}{2}a_E\left(T-T_{cE}^*\right)Q_E^2+\frac{1}{4}b_EQ_E^4 \quad (A.3)$$

$$e_6=-\frac{\lambda_{3E}Q_E}{C_{66}^o} \quad (A.4)$$

$$T_{cE}^*=T_{cE}+\frac{\lambda_{3E}^2}{a_EC_{66}^o} \quad (A.5)$$

$$C_{66}=C_{66}^o\left(\frac{T-T_{cE}^*}{T-T_{cE}}\right) \quad \text{at} \quad T>T_{cE}^* \quad (A.6)$$

$$C_{66}=C_{66}^o-C_{66}^o\left(\frac{(T_{cE}^*-T_{cE})}{2\left(T_{cE}^*-T\right)+\left(T_{cE}^*-T_{cE}\right)}\right) \quad \text{at} \quad T<T_{cE}^*. \quad (A.7)$$

Strain coupling effects associated with the normal—superconducting transition can be represented most simply as arising from a second order transition which is co-elastic in character. Assuming that strains other than e_6 (i.e. e_i with $i=1$–3) are negligibly small, the relevant Landau expansion is

$$G=\frac{1}{2}a_{SC}\left(T-T_c\right)Q_{SC}^2+\frac{1}{4}b_{SC}Q_{SC}^4+\lambda_{6SC}Q_{SC}^2e_6+\frac{1}{2}C_{66}^oe_6^2. \quad (A.8)$$

Note that, here, e_6 is the change in shear strain defined with respect to the orthorhombic parent structure whereas in equation (1) it is defined with respect to the tetragonal structure as reference state. The equilibrium condition $\partial G/\partial e_6=0$ gives

$$e_6=-\frac{\lambda_{6SC}}{C_{66}^o}Q_{SC}^2 \quad (A.9)$$

and substitution back into equation (A.8) gives

$$G=\frac{1}{2}a_{SC}\left(T-T_c\right)Q_{SC}^2+\frac{1}{4}b_{SC}^*Q_{SC}^4, \quad (A.10)$$

where

$$b_{SC}^*=b_{SC}-\frac{2\lambda_{6SC}^2}{C_{66}^o}. \quad (A.11)$$

The temperature dependence for C_{66} will be (following [126–128] and many others)

$$C_{66}=C_{66}^o \quad \text{at}\ T>T_c \quad (A.12)$$

and

$$C_{66}=C_{66}^o-\frac{2\lambda_{6SC}^2}{b_{SC}} \quad \text{at}\ T<T_c. \quad (A.13)$$

A.5. Strain analysis

In the absence of high resolution lattice parameter data for the specific sample used in the present study, data from the literature for samples with nearby compositions have been used to illustrate the form and magnitude of e_6 and e_1. With respect to a tetragonal reference structure, the symmetry-breaking shear strain, e_6, is given by

$$e_6 \approx \frac{2\,(a-b)}{(a+b)} = 2\delta \qquad \text{(A.14)}$$

where a and b are lattice parameters of the orthorhombic structure and δ is the strain parameter frequently used in the literature. A measure of e_1 is given by

$$e_1 = \frac{\Delta a}{a} - \left(\frac{\Delta a}{a}\right)_o \qquad \text{(A.15)}$$

where $\Delta a/a$ is the relative length change of a twinned single crystal of the orthorhombic phase in the [100] direction of the tetragonal para phase and $(\Delta a/a)_o$ is the relative change of the tetragonal crystal extrapolated to temperatures below T_S.

Thermal expansion data for the a parameter of a single crystal with $x = 0.045$ [48] are reproduced in figure A5. The coth function

$$\left(\frac{\Delta a}{a}\right)_o = a_1 + a_2\Theta_s \coth\left(\frac{\Theta_s}{T}\right), \qquad \text{(A.16)}$$

where a_1, a_2 and Θ_s are constants (e.g. [59]), has been fit in a temperature interval of ~80 K above T_S. The fit was then used to generate the variations of e_1 (equation (A.15)) shown in figure 6(a). Also given in figure 6(a) are values of e_6 extracted from data given by Nandi *et al* [6] for δ as a function of temperature for a sample with $x = 0.047$.

A.6. Symmetry adapted combinations of elastic constants

In order to consider the elastic constants in their diagonalised form, the eigenvalues and eigenvectors from the diagonalised elastic constant matrix for crystals with point group symmetry 4*mm*, $\bar{4}2m$, 422 and 4/*mmm* are given in table A2 (after [126]). As set out also in figure 2 of Yoshizawa *et al* [32] and Simayi *et al* [34], they show that a tetragonal crystal of $Ba(Fe_{1-x}Co_x)_2As_2$ is expected to have three discrete shear elastic constants. In symmetry-adapted form these are $\frac{1}{2}(C_{11} - C_{12})$, C_{66} and C_{44}. The other two combinations of elastic constants belong to irrep A_1.

A.7. Landau description for softening of C_{66} through T_c

Treating the evolution of C_{66} in terms of an effective coupling between Q_{SC} and e_6 through a second order transition described by equation (A.8) involves the assumption that the other strains are negligibly small in comparison. This appears to be the case for $x \sim 0.045$ ($e_1 \approx 0.000\,006$ when $e_6 \approx 0.0001$ in figure 6(a) above). The magnitude of the step-like softening C_{66} below T_c is then expected to follow equation (A.13). Values for the relevant Landau parameters can be estimated by first considering the heat capacity data for Crystal 2 which show a small step, $\Delta C_p \approx 0.05$ J · mole^{-1} · K^{-1}, at ~12.5 K [20]. This gives $a_{SC} = 2\Delta C_p \approx 0.1$ J · mole^{-1} · K^{-1} and b^*_{SC} $(=a_{SC}T_c) \approx 1.25$ J · mole^{-1} if T_c is taken as 12.5 K. Using the change in e_6 due to the normal—superconducting transition at $x = 0.047$ as being -0.0001 and an effective value of C^o_{66} for the orthorhombic reference state as ~30 GPa, gives $\lambda_{6SC} \approx 0.003$ GPa (Equation (A9)) and $b_{SC} \approx 1.29$ J · mole^{-1} (equation (A.11)). It follows, using the conversion between GPa and J · mole^{-1} from above, that $C^o_{66} - C_{66} \approx 0.86$ GPa (equation (A.13)), which represents softening by ~3%. Equivalent calculations starting with the heat capacity data of Hardy *et al* [47] for crystals with $x = 0.04$ ($\Delta C_p \approx 0.03$ J · mole^{-1} · K^{-1}, $T_C = 5.8$ K) and $x = 0.05$ ($\Delta C_p \approx 0.43$ J · mole^{-1} · K^{-1}, $T_C = 19.5$ K) predict softening by ~9% and ~0.2%, respectively. The observed softening below T_C at $x = 0.043$ is ~6%, showing that this simple parameterization provides a representation of the overall pattern of behaviour which is at least semi-quantitative.

Changes in C_{11} and C_{33} are expected to have the same form as C_{66} due to coupling with non-symmetry breaking strains e_1 and e_3 as $\lambda e Q^2_{SC}$, and small stepwise softening amounting to ~0.2%–0.3% is evident for both in the data of Goto *et al* [30]. Stepwise softening of C_{33} amounts to less than ~0.01% in the data of Simayi *et al* [34] for crystals with compositions in the range ~0.06–0.12. Softening shown by C_{11} in the data of Kurihara *et al* [42] is even smaller than this. Direct evidence of the strains themselves, such as for e_1 in figure 6(a) from the data of Meingast *et al* [48], is that this coupling is indeed weak.

Finally, the lack of any overt influence on resonances identified as being determined by C_{44} or $(\frac{1}{2}(C_{11} - C_{12})$ implies that the coefficients for coupling of the form $\lambda(e_1 - e_2)^2 Q^2_{SC}$ and $\lambda e_4^2 Q^2_{SC}$ are small. This is consistent with the pulse-echo ultrasonic data given by Goto *et al* [25] for a crystal with $x = 0.07$ (the original composition was specified as $x = 0.1$ but subsequently corrected [27]) and by Kurihara *et al* [42] for a crystal specified as having $x = 0.036$, which show only the slightest anomalies at T_c.

ORCID iDs

M A Carpenter https://orcid.org/0000-0003-2855-0007
A E Bohmer https://orcid.org/0000-0001-6836-2954
C Meingast https://orcid.org/0000-0002-3278-7544
P Mukherjee https://orcid.org/0000-0001-5121-6280

References

[1] Rotundu C R *et al* 2010 *Phys. Rev.* B **82** 144525
[2] Kim M G, Fernandes R M, Kreyssig A, Kim J W, Thaler A, Bud'ko S L, Canfield P C, McQueeney R J, Schmalian J and Goldman A I 2011 *Phys. Rev.* B **83** 134522
[3] Poirier M, Bilodeau M, Lefebvre S, Karki A B and Jin R 2014 *Phys. Rev.* B **89** 155129
[4] Forrest T R, Valdivia P N, Rotundu C R, Bourret-Courchesne E and Birgeneau R J 2016 *J. Phys.: Condens. Matter* **28** 115702
[5] Chu J-H, Analytis J G, Kucharczyk C and Fisher I R 2009 *Phys. Rev.* B **79** 014506
[6] Nandi S *et al* 2010 *Phys. Rev. Lett.* **104** 057006
[7] Pratt D K *et al* 2011 *Phys. Rev. Lett.* **106** 257001
[8] Rotundu C R and Birgeneau R J 2011 *Phys. Rev.* B **84** 092501
[9] Bernhard C *et al* 2012 *Phys. Rev.* B **86** 184509
[10] Salje E K H and Zhang H 2009 *Phase Trans.* **82** 452

[11] Salje E K H 2010 *ChemPhysChem* **11** 940
[12] Catalan G, Seidel J, Ramesh R and Scott J F 2012 *Rev. Mod. Phys.* **84** 119
[13] Salje E K H and Lashley J C 2012 *Disorder and Strain Induced Complexity in Functional Materials* (*Springer Series in Materials Science* vol 148) ed T Kakeshita *et al* (Berlin: Springer)
[14] Salje E K H and Carpenter M A 2015 *Phys. Status Solidi* b **252** 2639
[15] Kalisky B, Kirtley J R, Analytis J G, Chu J-H, Fisher I R and Moler K A 2011 *Phys. Rev.* B **83** 064511
[16] Prozorov R, Tanatar M A, Ni N, Kreyssig A, Nandi S, Bud'ko S L, Goldman A I and Canfield P C 2009 *Phys. Rev.* B **80** 174517
[17] Karahasanovic U and Schmalian J 2016 *Phys. Rev.* B **93** 064520
[18] Kuo H H, Chu J H, Palmstrom J C, Kivelson S A and Fisher I R 2016 *Science* **352** 958
[19] Iida K *et al* 2016 *Sci. Rep.* **6** 28390
[20] Evans D M, Schiemer J A, Wolf T, Adelmann P, Böhmer A E, Meingast C, Dutton S E, Mukherjee P, Hsu Y-T and Carpenter M A 2019 *J. Phys.: Condens. Matter* accepted
[21] Böhmer A E and Meingast C 2016 *C.R. Phys.* **17** 90
[22] Núñez-Regueiro M 2009 *Europhys. Lett.* **88** 37004
[23] Cano A, Civelli M, Eremin I and Paul I 2010 *Phys. Rev.* B **82** 020408
[24] Kuo H-H, Shapiro M C, Riggs S C and Fisher I R 2013 *Phys. Rev.* B **88** 085113
[25] Fernandes R M *et al* 2010 *Phys. Rev.* B **81** 140501
[26] Gallais Y, Fernandes R M, Paul I, Chauvière L, Yang Y-X, Méasson M-A, Cazayous M, Sacuto A, Colson D and Forget A 2013 *Phys. Rev. Lett.* **111** 267001
[27] Chu J-H, Kuo H-H, Analytis J G and Fisher I R 2012 *Science* **337** 710
[28] Fernandes R M, Chubukov A V and Schmalian J 2014 *Nat. Phys.* **10** 97
[29] Fernandes R M, VanBebber L H, Bhattacharya S, Chandra P, Keppens V, Mandrus D, McGuire M A, Sales B C, Sefat A S and Schmalian J 2010 *Phys. Rev. Lett.* **105** 157003
[30] Goto T, Kurihara R, Araki K, Mistumoto K, Akatsu M, Nemoto Y, Tatematsu S and Sato M 2011 *J. Phys. Soc. Japan* **80** 073702
[31] Yoshizawa M *et al* 2012 *J. Phys. Soc. Japan* **81** 024604
[32] Yoshizawa M and Simayi S 2012 *Mod. Phys. Lett.* B **26** 1230011
[33] Fernandes R M, Böhmer A E, Meingast C and Schmalian J 2013 *Phys. Rev. Lett.* **111** 137001
[34] Simayi S *et al* 2013 *J. Phys. Soc. Japan* **82** 114604
[35] Böhmer A E, Burger P, Hardy F, Wolf T, Schweiss P, Fromknecht R, Reinecker M, Schranz W and Meingast C 2014 *Phys. Rev. Lett.* **112** 047001
[36] Howard C J and Carpenter M A 2012 *Acta Crystallogr.* B **68** 209
[37] Khalyavin D D, Lovesey S W, Manuel P, Krüger F, Rosenkranz S, Allred J M, Chmaissem O and Osborn R 2014 *Phys. Rev.* B **90** 174511
[38] Salje E K H 1993 *Phase Transitions in Ferroelastic and Co-elastic Crystals* (Cambridge: Cambridge University Press)
[39] Carpenter M A, Zhang Z and Howard C J 2012 *J. Phys.: Condens. Matter* **24** 156002
[40] Zhang Z, Church N, Lappe S-C, Reinecker M, Fuith A, Saines P J, Harrison R J, Schranz W and Carpenter M A 2012 *J. Phys.: Condens. Matter* **24** 215404
[41] Carpenter M A, McKnight R E A, Howard C J and Knight K S 2010 *Phys. Rev.* B **82** 094101
[42] Kurihara R, Mitsumoto K, Akatsu M, Nemoto Y, Goto T, Kobayashi Y and Sato M 2017 *J. Phys. Soc. Japan* **86** 064706
[43] Carpenter M A 2015 *J. Phys.: Condens. Matter* **27** 263201
[44] Böhmer A E 2014 Competing phases in iron-based superconductors studied by high-resolution thermal-expansion and shear-modulus measurements *Doctoral Thesis* Karlsruher Institut für Technologie
[45] Hardy F, Adelmann P, Wolf T, Löhneysen H V and Meingast C 2009 *Phys. Rev. Lett.* **102** 187004
[46] Hardy F, Wolf T, Fisher R A, Eder R, Schweiss P, Adelmann P, Löhneysen H V and Meingast C 2010 *Phys. Rev.* B **81** 060501
[47] Hardy F *et al* 2010 *Europhys. Lett.* **91** 47008
[48] Meingast C, Hardy F, Heid R, Adelmann P, Böhmer A, Burger P, Ernst D, Fromknecht R, Schweiss P and Wolf T 2012 *Phys. Rev. Lett.* **108** 177004
[49] Ni N, Tillman M E, Yan J-Q, Kracher A, Hannahs S T, Bud'ko S L and Canfield P C 2008 *Phys. Rev.* B **78** 214515
[50] Prozorov R, Tanatar M A, Blomberg E C, Prommapan P, Gordon R T, Ni N, Bud'ko S L and Canfield P C 2009 *Physica* C **469** 667
[51] Prozorov R *et al* 2008 *Phys. Rev.* B **78** 224506
[52] Shen B, Cheng P, Wang Z, Fang L, Ren C, Shan L and Wen H-H 2010 *Phys. Rev.* B **81** 014503
[53] Inosov D S *et al* 2010 *Phys. Rev.* B **81** 014513
[54] Migliori A and Sarrao J L 1997 *Resonant Ultrasound Spectroscopy: Applications to Physics, Materials Measurements and Nondestructive Evaluation* (New York: Wiley)
[55] McKnight R E A, Carpenter M A, Darling T W, Buckley A and Taylor P A 2007 *Am. Mineral.* **92** 1665
[56] Schiemer J, Spalek L J, Saxena S S, Panagopoulos C, Katsufuji T, Bussmann-Holder A, Köhler J and Carpenter M A 2016 *Phys. Rev.* B **93** 054108
[57] Evans D M, Schiemer J A, Schmidt M, Wilhelm H and Carpenter M A 2017 *Phys. Rev.* B **95** 094426
[58] Bud'ko S L, Ni N, Nandi S, Schmiedeshoff G M and Canfield P C 2009 *Phys. Rev.* B **79** 054525
[59] Carpenter M A, Meyer H-W, Sondergeld P, Marion S and Knight K A 2003 *Am. Mineral.* **88** 534
[60] Huang Q, Qiu Y, Bao W, Green M A, Lynn J W, Gasparovic Y C, Wu T, Wu G and Chen X H 2008 *Phys. Rev. Lett.* **101** 257003
[61] Carpenter M A, Buckley A, Taylor P A and Darling T W 2010 *J. Phys.: Condens. Matter* **22** 035405
[62] Tanatar M A, Kreyssig A, Nandi S, Ni N, Bud'ko S L, Canfield P C, Goldman A I and Prozorov R 2009 *Phys. Rev.* B **79** 180508
[63] Carpenter M A, Sinogeikin S V and Bass J D 2010 *J. Phys.: Condens. Matter* **22** 035404
[64] Weller M, Li G Y, Zhang J X, Ke T S and Diehl J 1981 *Acta Metall.* **29** 1047
[65] Schaller R, Fantozzi G and Gremaud G 2001 *Mechanical Spectroscopy Q − 1 2001: With Applications to Materials Science* (Clausthal: TransTech. Publ.)
[66] Harrison R J and Redfern S A T 2002 *Phys. Earth Planet Inter.* **134** 253
[67] Harrison R J, Redfern S A T and Street J 2003 *Am. Mineral.* **88** 574
[68] Schranz W, Sondergeld P, Kityk A V and Salje E K H 2009 *Phys. Rev.* B **80** 094110
[69] Salje E K H and Zhang H 2009 *J. Phys.: Condens. Matter* **21** 035901
[70] Carpenter M A, Salje E K H and Howard C J 2012 *Phys. Rev.* B **85** 224430
[71] Carpenter M A, Howard C J, McKnight R E A, Migliori A, Betts J B and Fanelli V R 2010 *Phys. Rev.* B **82** 134123

[72] Cannelli G, Cantelli R, Cordero F, Trequattrini F and Ferretti M 1996 *Phys. Rev.* B **54** 15537
[73] Berciu M, Elfimov I and Sawatzky G A 2009 *Phys. Rev.* B **79** 214507
[74] Nowick A S and Berry B S 1972 *Anelastic Relaxation in Crystalline Solids* (New York: Academic)
[75] Thomson R I, Chatterji T and Carpenter M A 2014 *J. Phys.: Condens. Matter* **26** 146001
[76] Errandonea G 1980 *Phys. Rev.* B **21** 5221
[77] Martinelli A, Bernardini F and Massidda S 2016 *C. R. Phys.* **17** 5
[78] Böhmer A E, Hardy F, Wang L, Wolf T, Schweiss P and Meingast C 2015 *Nat. Commun.* **6** 7911
[79] Barzykin V and Gor'kov L P 2009 *Phys. Rev.* B **79** 134510
[80] Paul I 2011 *Phys. Rev. Lett.* **107** 047004
[81] Kuo H-H, Analytis J G, Chu J-H, Fernandes R M, Schmalian J and Fisher I R 2012 *Phys. Rev.* B **86** 134507
[82] Salje E K H and Carpenter M A 2011 *J. Phys.: Condens. Matter* **23** 462202
[83] Salje E and Devarajan V 1986 *Phase Trans.* **6** 235
[84] Migliori A, Sarrao J L, Visscher W M, Bell T M, Lei M, Fisk Z and Leisure R G 1993 *Physica* B **183** 1
[85] Salje E K H, Carpenter M A, Nataf G F, Picht G, Webber K, Weerasinghe J, Lisenkov S and Bellaiche L 2013 *Phys. Rev.* B **87** 014106
[86] Aktas O, Salje E K H, Crossley S, Lampronti G I, Whatmore R W, Mathur N D and Carpenter M A 2013 *Phys. Rev.* B **88** 174112
[87] Carpenter M A, Bryson J F J, Catalan G, Zhang S J and Donnelly N J 2012 *J. Phys.: Condens. Matter* **24** 045902
[88] Cantoni C, McGuire M A, Saparov B, May A F, Keiber T, Bridges F, Sefat A S and Sales B C 2015 *Adv. Mater.* **27** 2715
[89] Dioguardi A P *et al* 2013 *Phys. Rev. Lett.* **111** 207201
[90] Dioguardi A P *et al* 2015 *Phys. Rev.* B **92** 165116
[91] Shannon R D 1976 *Acta Crystallogr.* A **32** 751
[92] Carpenter M A, McKnight R E A, Howard C J, Zhou Q, Kennedy B J and Knight K S 2009 *Phys. Rev.* B **80** 214101
[93] Howard C J, Zhang Z, Carpenter M A and Knight K S 2007 *Phys. Rev.* B **76** 054108
[94] Wilson S D, Yamani Z, Rotundu C R, Freelon B, Bourret-Courchesne E and Birgeneau R J 2009 *Phys. Rev.* B **79** 184519
[95] Laplace Y, Bobroff J, Rullier-Albenque F, Colson D and Forget A 2009 *Phys. Rev.* B **80** 140501
[96] Marsik P *et al* 2010 *Phys. Rev. Lett.* **105** 057001
[97] Tanatar M A *et al* 2010 *Phys. Rev.* B **81** 184508
[98] Blomberg E C, Tanatar M A, Fernandes R M, Mazin I I, Shen B, Wen H H, Johannes M D, Schmalian J and Prozorov R 2013 *Nat. Commun.* **4** 1914
[99] Wenyuan S, Huimin S, Yening W and Baosheng L 1985 *J. Phys. Colloq.* **46** C10-609
[100] Yening W, Wenyuan S, Xiaohua C, Huimin S and Baosheng L 1987 *Phys. Status Solidi* a **102** 279
[101] Chrosch J and Salje E K H 1999 *J. Appl. Phys.* **85** 722
[102] Kityk A V, Schranz W, Sondergeld P, Havlik D, Salje E K H and Scott J F 2000 *Europhys. Lett.* **50** 41
[103] Niedziela J L, Parshall D, Lokshin K A, Sefat A S, Alatas A and Egami T 2011 *Phys. Rev.* B **84** 224305
[104] Gofryk K, Sefat A S, McGuire M A, Sales B C, Mandrus D, Thompson J D, Bauer E D and Ronning F 2010 *Phys. Rev.* B **81** 184518
[105] Allan M P *et al* 2013 *Nat. Phys.* **9** 220
[106] Bag B, Vinod K, Bharathi A and Banerjee S S 2016 *New J. Phys.* **18** 063025
[107] Zou Q *et al* 2017 *Nano Lett.* **17** 1642
[108] Li L *et al* 2017 *Sci. Rep.* **7** 949
[109] Sun D L, Xiao J Z and Lin C T 2011 *J. Cryst. Growth* **321** 55
[110] Gofryk K, Vorontsov A B, Vekhter I, Sefat A S, Imai T, Bauer E D, Thompson J D and Ronning F 2011 *Phys. Rev.* B **83** 064513
[111] Kim Y K *et al* 2013 *Phys. Rev. Lett.* **111** 217001
[112] Ma C, Wu L, Yin W-G, Yang H, Shi H, Wang Z, Li J, Homes C C and Zhu Y 2014 *Phys. Rev. Lett.* **112** 077001
[113] Arham H Z *et al* 2012 *Phys. Rev.* B **85** 214515
[114] Kretzschmar F *et al* 2016 *Nat. Phys.* **12** 560
[115] Aird A and Salje E K H 1988 *J. Phys.: Condens. Matter* **10** L377
[116] Li B, Li J, Bassler K E and Ting C S 2013 *New J. Phys.* **15** 103018
[117] Kirtley J R, Kalisky B, Luan L and Moler K A 2010 *Phys. Rev.* B **81** 184514
[118] Kalisky B, Kirtley J R, Analytis J G, Chu J-H, Vailionis A, Fisher I R and Moler K A 2010 *Phys. Rev.* B **81** 184513
[119] Tranquada J M 2010 *Physics* **3** 14
[120] Avci S *et al* 2011 *Phys. Rev.* B **83** 172503
[121] Avci S *et al* 2014 *Nature Commun.* **5** 3845
[122] McQueen T M, Williams A J, Stephens P W, Tao J, Zhu Y, Ksenofontov V, Casper F, Felser C and Cava R J 2009 *Phys. Rev. Lett.* **103** 057002
[123] Böhmer A E, Arai T, Hardy F, Hattori T, Iye T, Wolf T, Löhneysen H V, Ishida K and Meingast C 2015 *Phys. Rev. Lett.* **114** 027001
[124] Stokes H T, van Orden S and Campbell B J 2016 *J. Appl. Cryst.* **49** 1849
[125] Stokes H T, Hatch D M and Campbell B J ISOTROPY software suite (http://stokes.byu.edu/isotropy.html)
[126] Carpenter M A and Salje E K H 1998 *Eur. J. Mineral.* **10** 693
[127] Slonczewski J C and Thomas H 1970 *Phys. Rev.* B **1** 3599
[128] Rehwald W 1973 *Adv. Phys.* **22** 721